EFFECTIVE THERMAL CONDUCTIVITY OF AN ALUMINUM FOAM+WATER TWO PHASE SYSTEM

A Thesis
Presented To
The Faculty Of The Department Of Materials Engineering
San Jose State University

In Partial Fulfillment
Of The Requirements For The Degree
Master Of Science

By
John Moskito
December 1996

APPROVED FOR THE DEPARTMENT OF
MATERIALS ENGINEERING

Dr. Guna Selvaduray

Dr. Bruce Webbon, NASA-Ames Research Center

Dr. XXXX XXXXXX

APPROVED FOR THE UNIVERSITY

UMI Abstract

ABSTRACT

EFFECTIVE THERMAL CONDUCTIVITY OF AN

ALUMINUM FOAM + WATER SYSTEM

by John Moskito

This study examined the effect of volume fraction and pore size on the effective thermal conductivity of an aluminum foam and water system. Nine specimens of aluminum foam representing a matrix of three volume fractions (4-8% by vol.) and three pore sizes (2-4mm) were tested with water to determine relationships to the effective thermal conductivity. It was determined that increases in volume fraction of the aluminum phase was correlated to increases in the effective thermal conductivity. It was not statistically possible to prove that changes in pore size of the aluminum foam correlated to changes in the effective thermal conductivity. However, interaction effects between the volume fraction and pore size of the foam were statistically significant. Ten theoretical models were selected from the published literature to compare against the experimental data. Models by Asaad, Hadley [1986], and de Vries provided effective thermal conductivity predictions within a 95% confidence interval.

Acknowledgments

The author would like to acknowledge the following people. For without their sponsorship, guidance, and assistance this work would not have been possible.

Dr. Bruce Webbon, Branch Chief, Advanced Life Support - NASA-Ames Research Center, whose funding and laboratory facilities made this work possible.

Curt Lomax, Advanced Life Support - NASA-Ames Research Center, who first proposed the project. Curt provided guidance, expertise, friendship and enthusiasm.

Dr. Guna Selvaduray, San Jose State University, who patiently guided me towards completion of the project.

This work is dedicated to Megan, who has stood by me throughout.

Introduction

In the United States of America, the exploration of space has been divided into five programs: Mercury and Gemini, laid the groundwork for future exploration; Apollo visited the Moon; Skylab established a long-term presence in space; and the current Shuttle program focuses on short-term, Low Earth Orbit-based missions. The next program for the United States is the International Space Station, which will provide a base for a continuous multi-national presence in space.

A common thread among each of these space programs is the use of astronauts, outside of their spacecraft, in a self-sufficient, self-contained capacity, who conduct experiments, perform maintenance and repairs, and explore new worlds. The technology that allows these astronauts to perform in space is directly related to the environment each program encounters.

Extravehicular Activity

When the astronaut leaves the spacecraft to perform a task he performs an Extravehicular Activity (EVA). Alexei A. Leonov and Edward

H. White were the first Soviet and American astronauts, respectively, to perform EVA's. White ventured from his Gemini capsule on June, 3 1965. His spacewalk lasted about one-half hour. (Ref. 1)

Over the course of the Gemini program, astronauts logged 12 more hours of EVA time. In later programs, even more EVA hours were logged. One hundred sixty-five hours were spent outside the spacecraft during the Apollo program. Of those hours, 161 were spent walking on the surface of the moon. The Skylab program added 82 more EVA hours. (Ref. 2) Space Shuttle astronauts have logged hundreds hours of EVA time. (Ref. 3)

There is a continuing need for astronauts to "Go EVA". Mobility outside and away from the ship is required for repair and maintenance of the craft itself. Sixty-five hours of unscheduled EVA were conducted during the Skylab program to repair damage the space station suffered during deployment. Conducting experiments and the repair and service of satellites and other space hardware will require astronauts to venture outside the spacecraft. The building of the International Space Station is anticipated to require hundreds of EVA-hours. (Ref. 4)

Components of a space suit

When an astronaut ventures outside the protective environs of the spaceship he/she must take along an environment that will provide the life support systems needed to survive. During an EVA the astronaut wears a number of life support items that are collectively termed the Extravehicular Mobility Unit (EMU).

There are 19 separate systems, or modules, that make up the current Shuttle spacesuit or EMU. (Ref. 1) These systems are shown in Figure 1. The

Shuttle EMU systems provide the astronaut with pressure, thermal insulation, and micrometeorite protection. Oxygen, climate control, drinking water, food, and waste collection are all provided within the suit. Electrical power and communications equipment are also supplied. Table 1 provides a breakdown of the EMU equipment and lists their primary uses.

Spacesuit improvements

The Shuttle EMU provides an excellent basis from which to perform Low-Earth Orbit (LEO) EVA's. However, suit requirements for the for the International Space Station (ISS) may necessitate changes to some of the current Shuttle EMU systems due to the long mission duration and multiple EVA scenarios envisioned during the construction and occupancy phases of the ISS.

Changes envisioned for the Shuttle EMU to enable it to be used as an International Space Station EMU include increasing suit pressure to 8.3 psia, allowing the capability to resize and service the EMU in orbit, and conserving cooling water that is vaporized in the suit's thermal regulation

sub-system during EVA. Current suit pressure is 4.3 psia but the shuttle cabin pressure is 8.3 psia. The difference in pressures requires a lengthy pre-breathe period prior to EVA to acclimate the astronaut to the reduced suit pressure. By constructing a suit designed for an 8.3 psia pressure, the pre-breathe time can be saved.

Table 1. Shuttle EMU Item List (From Ref. 1)

Item	Description	Item	Description
Portable Life-Support System (PLSS)	Provides oxygen, CO_2 removal, warning system, electrical power, water cooling system, and radio	Display and Control Module (DCM)	Contains all controls, digital display, and external interfaces
EMU Electrical Harness (EEH)	Provides bio-instrumentation and communications connections to PLSS	Secondary Oxygen Pack	Supplies 30-minute emergency supply
Service & Cooling Umbilical (SCU)	Provides interface between EMU and orbiter	Battery	Supplies electrical power
Contaminant Control Cartridge (CCC)	Cleanses suit atmosphere	Hard Upper Torso (HUT)	Upper torso of suit
Lower torso	Suit pants	Arms (left and right)	
EVA Gloves	Tool tethers and wristwatch built-in	Helmet	Plastic pressure bubble
Liquid Cooling Garment (LCG)	Provides cooling water	Urine Collection Device (UCD)	Urine collection for male crew members
Disposable Absorption and Containment Trunk (DACT)	Urine collection for female crew members	Extravehicular Visor Assembly (EVA)	Provides sun-filterin visor, headlamps, and TV camera-transmitter
In-Suit Drink Bag (IDB)	Provides drinking water for crew member	Communications Carrier Assembly (CCA)	Porvides earphones and microphone for crew member
Airlock Adapter Plate (AAP)	Provides mounting and storage fixture for suit		

The ability to resize the suit in orbit would allow greater flexibility in crew selection and EVA work schedules. In-orbit servicing of the Space Station EMU will be required for crew members and their EMU's staying in

orbit for weeks or months at a time. Current EMU design restricts a suit to 21 hours of use before return to Earth for complete cleaning and re-certification, (Ref. 1, 4) which is not amenable to Space Station service.

In the current Shuttle EMU design, cooling water used for thermal regulation of the suit is not conserved. To remove metabolic heat generated by the astronaut water is sublimated into the vacuum of space. Up to 5.44 kg (12 lb.) of water can be vaporized into space with each 8-hour EVA. (Ref. 5, 6) Eliminating this loss of water during EVA will conserve a resource that is precious in a space environment.

An alternative technology for ISS EMU thermal regulation

Thermal regulation for the spacesuit consists primarily of removing metabolic heat generated by the astronaut from the body area of the suit. The thermal regulating system collects, transports, then either stores or removes this heat.

An alternative technology for the ISS EMU, proposed by the NASA-Ames Advanced Life Support Branch, is the Direct Interface Fusible Heat Sink (DIFHS). (Ref. 7, 8, 9) The system offers a system to store the metabolic heat generated by the astronaut. Storage is possible due to the absorption of the metabolic heat as a rise in the temperature of and a phase change in the DIFHS material. The DIFHS medium is water, that changes from ice (solid) to water (liquid) during use. By storing the heat for expulsion after the conclusion of the EVA, no resources, such as water, are expended during the EVA. Expulsion of the heat is accomplished after the completion of the EVA by freezing, or regenerating, the DIFHS water for the next EVA. This offers the advantage of eliminating the sublimation system used in the Shuttle EMU, thereby conserving the water that would have be sublimated into

space each EVA. The use of the Direct Interface Fusible Heat Sink for thermal regulation of the EMU in multiple-EVA sorties conserves resources compared to the Shuttle spacesuit sublimator unit.

A full description of the Direct Interface Fusible Heat Sink will be presented in the Background section but in general terms the DIFHS absorbs metabolic heat by passing cooling water across the astronaut's body, transports the absorbed heat by pumping the water to the backpack area of the EMU, then allows the now warm water to directly contact and transfer the absorbed heat to the DIFHS material. The DIFHS material, which is ice, increases in temperature, then melts, in order to accept the metabolic heat. At start-up, the transporting water must melt a passage through the DIFHS ice to form a channel through which the water may flow continuously during the remainder of the EVA. After the EVA, the DIFHS is removed from the EMU backpack, placed in a freezer, and refrozen for use in an up-coming EVA.

The two disadvantages of the DIFHS related to this work were inconsistent heat transfer rates in the melted channel during use and long refreezing times during regeneration. (Ref. 7, 8)

Heat transfer within the DIFHS is primarily a function of the mixing of the inlet water and the ice block inside the DIFHS. (Ref. 7) Experiments performed by Webbon and Lomax found at flow initiation, heat transfer rates were high. After a time, the heat transfer rate would drop due to coring through the block. Coring occurred after the water had melted a passage through the ice. Laminar flow through the passage insulated the inner core of water which contributed to reduced heat transfer rates. (Ref. 7)

Regeneration of the DIFHS consists of removal of the tank from the PLSS system to re-freeze the water in a freezer. In a 1-g environment, freezing is enhanced by natural convection caused by temperature-induced density gradients within the container. Convection allows the physical transport of cold water away from the container walls and its replacement with warmer water from the center. In a micro-gravity situation density changes are not accompanied by convection, hence the transport of heat from the center must be accomplished by thermal conduction alone. (Ref. 8, 10) As will be shown in the next section, the reliance on thermal conduction alone may exceed the allowable time period.

A possible solution to the disadvantages of uneven heat transfer during use and a long regeneration time afterwards is the introduction of an interlaced material into the DIFHS container. This material would be in intimate contact with the fusible medium and the container walls to provide thermal pathways for improved heat conduction. Heat transfer during use would be increased due to the heat exchange between the fusible media, the interlaced material, and the flow stream. Long regeneration times would be reduced by increasing the effective thermal conductivity of the material, both in the liquid and solid (ice) phases.

A possible candidate for use as an interlaced material in the DIFHS is an aluminum foam. (Ref. 8) This foam possesses an continuous open-pore matrix structure and a high thermal conductivity. Open pores allow the efficient flow of the fluid stream through the DIFHS. A continuous matrix aids in structure stability. These attributes can be seen in the foam image shown in Figure 2. The high thermal conductivity relative to water, which is the fusible medium, provides the increased heat transfer properties needed to

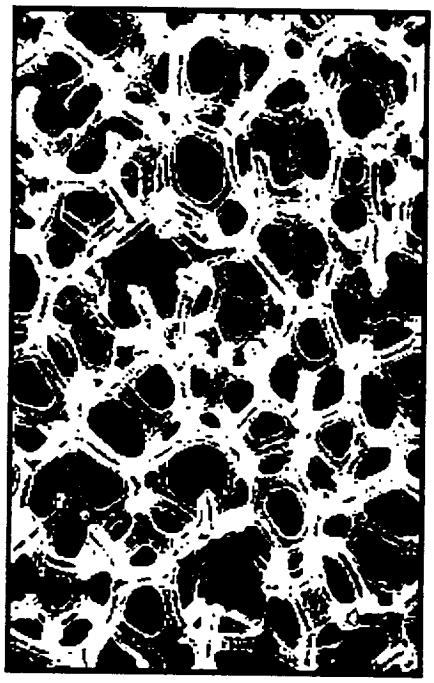

Figure 2. Aluminum foam as a candidate interlaced material (Photo courtesy of NASA-Ames Advanced Life Support Branch)

reduce the disadvantages of coring and long regeneration times in the DIFHS.

The improvement to the heat transfer properties to the DIFHS system with the addition of the aluminum foam can be estimated from empirical correlation equations. The heat transfer coefficient for the addition of the aluminum foam into the fluid stream can be estimated to a first approximation as a bank of staggered aluminum rods. The estimation of the heat transfer by this method provides a reliable means to predict the benefit attained in using an interlaced material.

The effective thermal conductivity is the sum of the combined thermal conductivities of the water and aluminum foam. The estimation of the

effective thermal conductivity, compared to the heat transfer, is not as well established or consistent. (Ref. 11, 12) As will be detailed in the next section, the empirical prediction of the effective thermal conductivity can vary as much as an order of magnitude based on the orientation of the materials and their relative thermal conductivities. Therefore, the effective thermal conductivity is confirmed typically by experiment.

This study measured the effective thermal conductivity of nine sets of aluminum foam and water . It was postulated that the addition of the aluminum foam would increase the effective thermal conductivity of the DIFHS system, thereby decreasing the time required for regeneration.

The next section of this report will review the cooling requirements for the Shuttle EMU and the proposed use of the Direct Interface Fusible Heat Sink as a replacement technology for the current sublimator for thermal regulation. The use of aluminum foam as a medium for increasing the effective thermal conductivity of the system will be examined with emphasis on a selection of models that predict the effective thermal conductivity.

Background

This chapter is divided into four sections; first, EMU thermal regulation subsystem requirements and the use of the Direct Interface Fusible Heat Sink as a potential technology for the ISS EMU are discussed. Second, the effect of using an interlacing material, such as the aluminum foam in this study, to improve heat transfer rates are examined. Equations are developed to predict the benefit of an interlacing material in the DIFHS. Third, the relevance of using effective thermal conductivity models from the published literature is discussed, and fourth, an overview of the issues concerning the experimental measurement of the effective thermal conductivity of a solid/liquid system is presented.

Thermal regulation subsystem performance requirements

Metabolic heat generated by the astronaut during an EVA is the primary source of heat the cooling system must remove from the body area. About 100 watts (400 BTU/hr) of heat is produced by an astronaut at rest. This heat output can be easily increased by an order of magnitude during periods of heavy work. (Ref. 6, 7, 8) Current total capacity requirements are 3420 watts (11680 BTU/hr) for an 8-hour EVA with a maximum cooling capacity of 585.5 watts (2000 BTU/hr) for any 15 minute period. (Ref. 8) Table 2 lists the cooling requirements for a Low Earth Orbit EVA regulation system.

Additional heat sources and sinks exist which include heat generated by the life support equipment and external sources. The average heat load

Table 2. Cooling Requirements for a Low Earth Orbit EVA (From Ref. 8)

EVA Duration	8 hours
EVA Environment	LEO (any Orientation)
Minimum Heat Load	117.1 Watt (400 BTU/hr)
Maximum Heat Load	585.6 Watt (2000 BTU/hr)
Total Heat Capacity	3420 Watt-hr (11680 BTU)
Outlet Temperature	<15.6°C (60°F)
Regeneration Time	<16 hours
EVA Frequency	8 hours/day, 6 days/week
Mission Duration	6 months
Operational Life	1228 hours

generated by the life support equipment in the PLSS is 186 watts (635 BTU/hr). (Ref. 7, 8, 10)

The astronaut's overall heat balance is affected by the ambient conditions encountered during the EVA. External heat transfer to and from the suit are mainly through radiation. Infrared energy can be absorbed from the sun, Earth, and nearby hot structures such as the payload bay of the shuttle. The astronaut simultaneously radiates energy into deep space.

Additional heat transfer to/from the suit can occur via conduction through contact with objects such as structures, tools, and equipment. Contact with the lunar or Martian surface during planetary missions will also impose a heat load (positive or negative) on the astronaut.

Convective heat transfer is also possible in certain situations. Mars has an atmosphere in which convective heat transfer will play a significant part of the total heat load equation.

Components of the thermal regulation system

The thermal regulation system is composed of three processes: 1) acquisition of the thermal energy from its sources (metabolic, instrumentation, ambient, etc.); 2) transport of the energy through the system; and 3) storage and/or removal of the heat from the suit environment.

The acquisition of metabolic heat is accomplished by use of the Liquid Cooling Garment (LCG). The LCG is worn against the body under the spacesuit. The LCG is a Spandex™ garment laced with tubing within which the cooling water is circulated. The LCG garment is shown in Figure 3. (Ref. 1, 2)

Heat transportation to and from the LCG and within the EMU is accomplished by pumping the cooling water through the system.

Storage/removal of the energy delivered by the water transportation system can be accomplished by a number of technologies. The current process of sublimating the heat into the vacuum of space has been proven over years of service to be an economical and reliable system for use in the Shuttle EMU. Possible heat storage and/or removal technologies for use in an ISS EMU include heat pipe/radiators, evaporative membranes, and the aforementioned Direct Interface Fusible Heat Sink. (Ref. 6, 9)

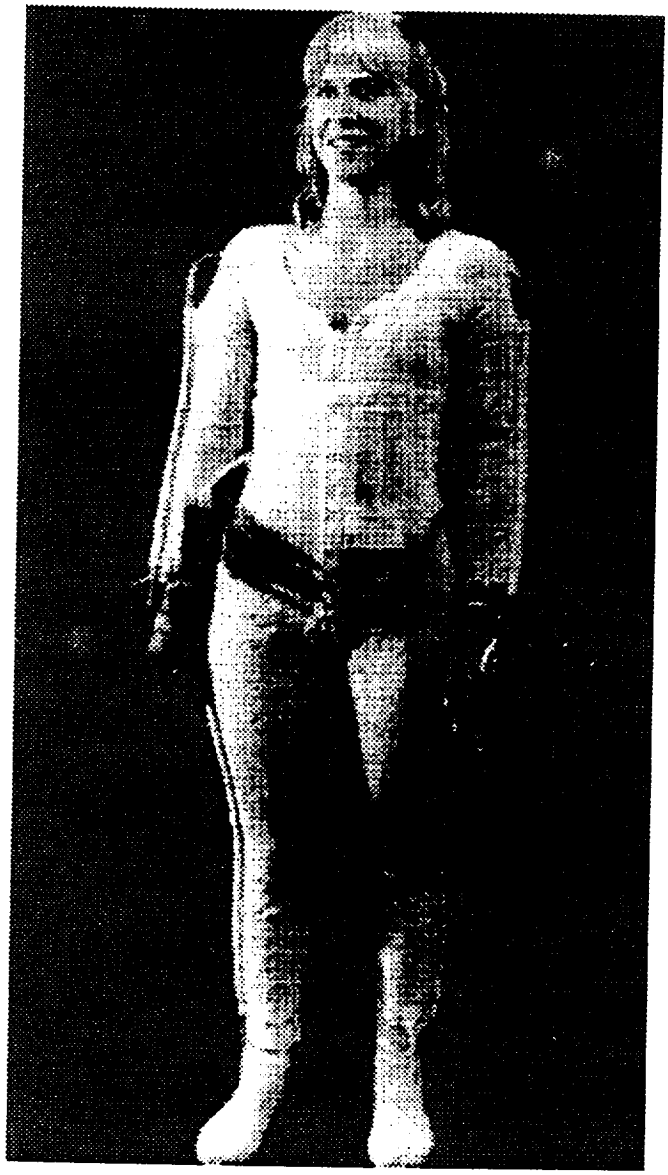

Figure 3. Liquid Cooling Garment, (LCG) (From Ref. 1)

Current NASA Shuttle EMU's utilize a flat plate sublimator as the heat removal unit. A schematic of the flat plate sublimator is shown in Figure 4. The sublimator unit is comprised of three main sections; a porous stainless steel plate, a feed-water channel located below the plate, and the LCG water loop. One side of the porous plate is vented to the vacuum of space. The

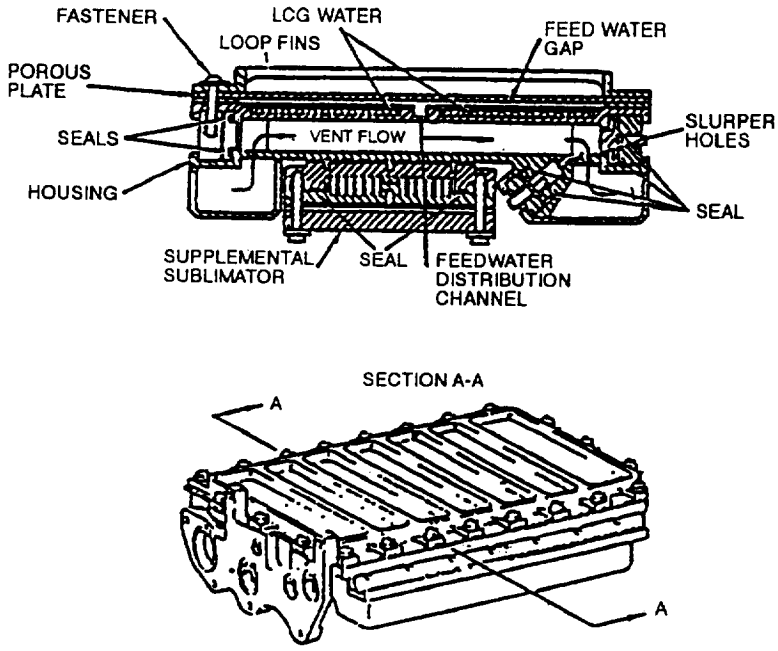

Figure 4. Flat Plate Sublimator (From Ref. 5)

other side is connected to the feed-water channel. Water pumped from the feed-water channel is allowed to percolate into the porous metal plate. A phase transformation occurs as the water "sees" the vacuum on the far side of the plate. The feed-water may freeze in the pores of the stainless plate and then evaporate/sublimate. The phase transformation cools the remaining water in the feed-water channel which in turn absorbs heat from the LCG coolant -water loop. (Ref. 5, 6, 13)

Advantages/disadvantages of the sublimator

The flat plate sublimator currently used in the NASA Shuttle suit has advantages and deficiencies compared to alternative cooling systems. Unit

weight and size are advantages to the sublimator. Mass depletion, fouling of the porous plate, and a required maximum pressure for sublimation are the flat plate sublimator's three main deficiencies.

The flat plate sublimator possesses the advantage of in-use replenishment of its fusible material (feed-water) and a compact size within the PLSS. The sublimator requires a 5.12 kg (12 lbm) supply of feed water for sublimation cooling for an 8-hour EVA. (Ref. 5) This feedwater supply is augmented during the EVA by water vapor condensed from the perspiration and exhaled air of the astronaut. (Ref. 1) This allows the sublimator system to extend its usable supply and/or maintain reserves for emergency use.

The largest component of the sublimator is the flat porous stainless steel plate. This plate presents an area of approximately 930 cm^2 (1 ft^2) towards the vacuum of space. In comparison to most alternative cooling systems, the flat plate sublimator has the advantage in weight and overall size.

The disadvantages of the flat plate sublimator are the loss of feed-water, fouling of the porous metal plate, and the inability to operate above a maximum ambient pressure. During use the feed-water is constantly sublimated into space. This mass cannot be recaptured. Multiple-EVA orbital missions such as during the construction phase of the International Space Station and long-duration missions which include lunar missions and Space Station assignments will be required to carry a large supply and/or source of feed-water for sublimator use.

Fouling or clogging of the porous metal plate with prolonged use is also a possible problem. Scheduled servicing of the sublimator plate will be

required for long-duration missions. The sublimator is restricted to 21 hours of use before return to Earth for complete cleaning and re-certification, (Ref. 4, 5)

The sublimation of solid water (ice) to vapor requires that the low-pressure side of the sublimator be below the triple point of water which is 0.088 psia at 32°F. The thermal environment of Mars consists of an atmosphere whose total pressure is approximately 0.08 psia and a surface temperature which can range from -130 to +40°F dependent on location and season. (Ref. 6) Therefore, because of the higher pressures that may be encountered, the flat plate sublimator would not be suitable for a Mars expedition.

Alternatives to the sublimator system

There are several alternative cooling systems to the flat plate sublimator of which the Heat pipe/Radiator, Evaporative Membrane Heat Exchanger, and Direct Interface Fusible Heat Sink are primary technologies. These systems offer both advantages and compromises over the current flat plate sublimator system.

Heat pipe/radiator technology uses a vaporizing fluid such as liquid nitrogen or ammonia to transport metabolic heat to radiator plates placed on the outside of the suit backpack. The heat pipe fluid absorbs heat from the LCG water loop and vaporizes. A thermal gradient along the heat pipe causes the vapor to travel to the radiator end where it condenses. The radiators eject the transported heat into deep space. The condensed fluid circulates back to the vaporizing end of the heat pipe by capillary action

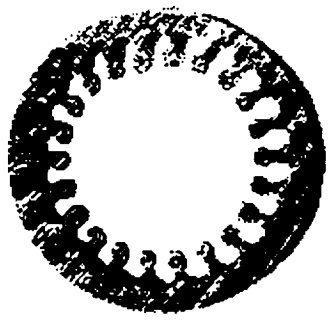

Figure 5. Heat Pipe Cross-Section with Re-Entrant Grooves (From Ref. 14)

along re-entrant grooves. (Ref. 14, 15) The cross-section of a heat pipe tube in Figure 5 shows the re-entrant grooves around the inner diameter.

The heat pipe/radiator system takes advantage of the 7.2°K (4°R) deep space radiation sink temperature by exposing a large area to space. However, radiators sized to handle the maximum heat loads anticipated during EVA would be prohibitively large. (Ref. 6) Use of a radiator-based system for EVA use would probably be sized for average EVA heat loads and coupled with a "top-off" cooling system, such as a sublimator or evaporative membrane heat exchanger, to handle the higher heat loads during strenuous astronaut activity.

Evaporative Membrane Heat Exchanger

The Evaporative Membrane Heat Exchanger ejects metabolic heat into space by boiling or vaporizing a small portion of the LCG water through a polymeric membrane. The Evaporative Membrane uses a membrane that is

impervious to liquid water but allows water vapor to pass through. The opposite side of the membrane is exposed to the vacuum of space. LCG water is pumped past the membrane the low pressure on the opposite side causes the water next to the membrane to evaporate or boil. The energy required to vaporize this water is taken from the remaining LCG water behind it. The now vaporized water can escape through the membrane into space. The remaining LCG water is pumped back to the Liquid Cooling Garment. The vaporization of water is controlled by controlling the partial pressure of water on the vacuum side of the membrane. In preliminary form the membrane is formed as a tube with the liquid water on the outside and the inner side vented to space. The partial pressure is controlled by sizing the inner tube diameter to match the diameter for choked flow through an orifice. (Ref. 16, 17, 18) Figure 6 shows a prototype version of the Evaporative Membrane.

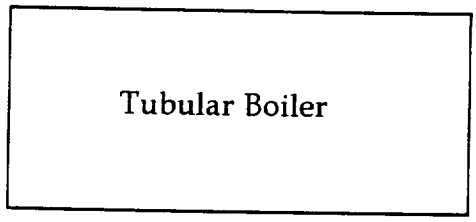

Figure 6. Evaporative Membrane
(Photo by author)

The Evaporative Membrane promises to substantially reduce the overall size and mass of the thermal regulating unit compared to the current flat plate sublimator. The Evaporative Membrane uses a membrane surface area approximately 85% smaller and 90% lighter than the flat plate sublimator. The feed-water loop is discarded resulting in additional weight and mass savings due to direct use of the LCG water as the phase

transformation medium. Since the Evaporative Membrane uses the latent heat of vaporization as the cooling source, higher atmospheric (vacuum) pressures can be endured. Atmospheric pressures up to the equilibrium vapor pressure at the LCG water temperature, which is typically 20°C (68°F), are possible. This higher pressure ceiling allows the Evaporative Membrane to be a candidate for a Mars expedition suit.

The disadvantages of the Evaporative Membrane result from its development as a new technology. The reliability of the polymer membrane in a space environment is not known in this time and the practical problem of controlling the partial pressure on the vacuum side requires further study.

Direct Interface Fusible Heat Sink

The Direct Interface Fusible Heat Sink (DIFHS) stores the metabolic heat generated by an astronaut. The heat is stored by using the heat of fusion to transform a suitable material from one phase to another. Such a suitable phase change material is water from solid (ice) to liquid. The liquid water is refrozen during a system regeneration after the EVA is completed. The DIFHS is unique in that the fusible material, water, is also the medium used to transport the heat from the garment to the PLSS. Through direct interface, or contact, of the LCG water and the DIFHS ice, cooling by forced convection as well as phase transformation can be obtained. (Ref. 7, 8)

The DIFHS has advantages that make it an viable alternative to the flat plate sublimator. Water is conserved so multiple-EVA operations become more economical. The DIFHS can be regenerated for additional EVA sorties on-board. Additionally, the large ice mass required for an 8-hour EVA is not a hindrance in micro-gravity (orbital) EVA scenarios. (Ref. 7)

The relatively low heat of fusion of water requires that a large mass of ice/water be carried by the astronaut. While not an important issue for micro-gravity EVA's, the DIFHS may not be an acceptable alternative for a Mars expedition due to the relatively large gravitational force there. (Ref. 7)

A selection of alternative methods for cooling an astronaut during EVA have been presented. For use in the International Space Station EMU, the DIFHS may provide the best choice in an alternative method due to its capability for no expendables and in-flight regeneration. The next few sections will develop the capacity requirements required for the DIFHS and the use of an interlaced material to assist in the heat transfer to and from the system.

Heat transfer

The mass of water required for a full sized DIFHS can be calculated. With a total cooling capacity of 3420 W-hr (11680 Btu) required for an 8-hour EVA, a DIFHS starts with ice initially cooled to -17.8°C (0°F) which melts, then warms to 4.4°C (40°F). With heat capacities, Cp, of ice and water of 2.052 Joule/°C gm and 4.216 Joule/°C gm, respectively, and a heat of fusion of 333.7 Joule/gm, the mass of water can be calculated from Equation [1]:

$$q = mCp_{ice}\Delta T_{ice} + mL + mCp_{water}\Delta T_{water} \qquad [1]$$

Therefore, a full sized DIFHS would hold approximately 31.7 kg (70 lb.) of water . The volume equivalent to this is 0.032 m^3 (1.12 ft^3) of water or 0.035 m^3 (1.25 ft^3) of ice. (Ref. 7, 8)

Prototype DIFHS units have been developed and tested at NASA-Ames Research Center. (Ref. 7, 8) One prototype is a $^1/_3$ scale DIFHS and is shown in the Figure 7. Design issues addressed in the DIFHS prototypes

have included measurement s of the heat transfer rate during use and the time required for regeneration.

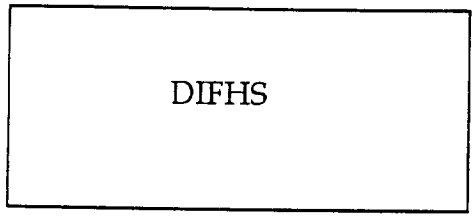

Figure 7. Direct Interface Fusible Heat Sink (Photo by author)

Incons istent heat transfer during use and long regeneration times to freeze the melt water are the major development issues for the DIFHS. In experiments by Lomax and Webbon (1990), after the initialization of flow through the DIFHS, heat transfer between the fluid stream and the surrounding ice decreased due to inadequate fluid mixing. Attempts to increase the turbulence of the fluid stream resulted in increased heat transfer rates. (Ref. 7) Later work by Lomax and Kader (1994) measured the regeneration time of a 1/2 scale DIFHS unit at 17 hours. (Ref. 8) Possible solutions proposed in these studies include baffling the interior of the tank with fins or using an interlaced material.

Baffles

Baffling the tank with cooling fins could increase the conduction surface area for heat transfer and allow passage of the LCG water flow without large penalties in pressure. (Ref. 7) On the downside, baffles require mass and volume increases to the overall DIFHS system. Baffling could also slow or prevent flow initiation due to long passages between inlet

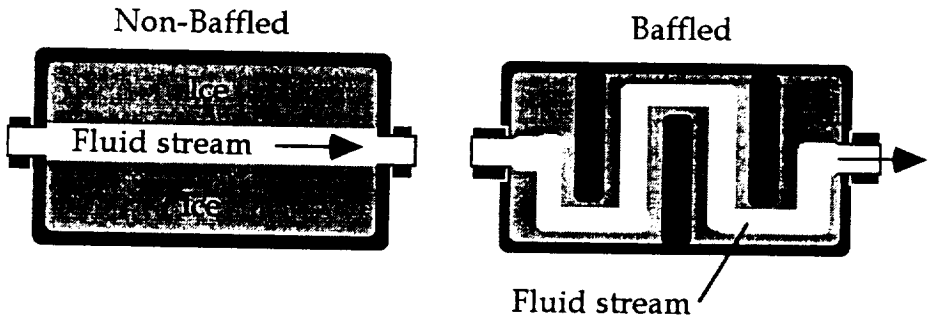

1.;Figure 8. Fluid streams through Non-Baffled and Baffled tanks

and outlet couplings. Additionally, channeling may still occur in a baffled tank. (Ref. 7)

The increased heat transfer that could be obtained using baffles can be estimated to a first approximation by using a simple laminar forced convection flow model. Assuming the LCG water melts, then flows, through a passage of constant circular cross section, the heat transfer within the DIFHS can be modeled as a simple flow through a tube. Figure 8 illustrates both the non-baffled tank and one with a baffle which increases the flow stream's length. In the baffled model the total length of the melt passage was assumed to be double the unbaffled model.

A maximum mass flow rate of 240 lb/hr for the LCG water system was used to determine the laminar flow regime. (Ref. 8) The average heat transfer coefficient, $\bar{h}$, was calculated from the average Nusselt number. The Hausen equation (Ref. 19) for a constant wall temperature provides the average Nusselt number. This equation is presented below as Equation [2].

$$\bar{h} = \overline{Nu}_D \frac{k}{D}$$

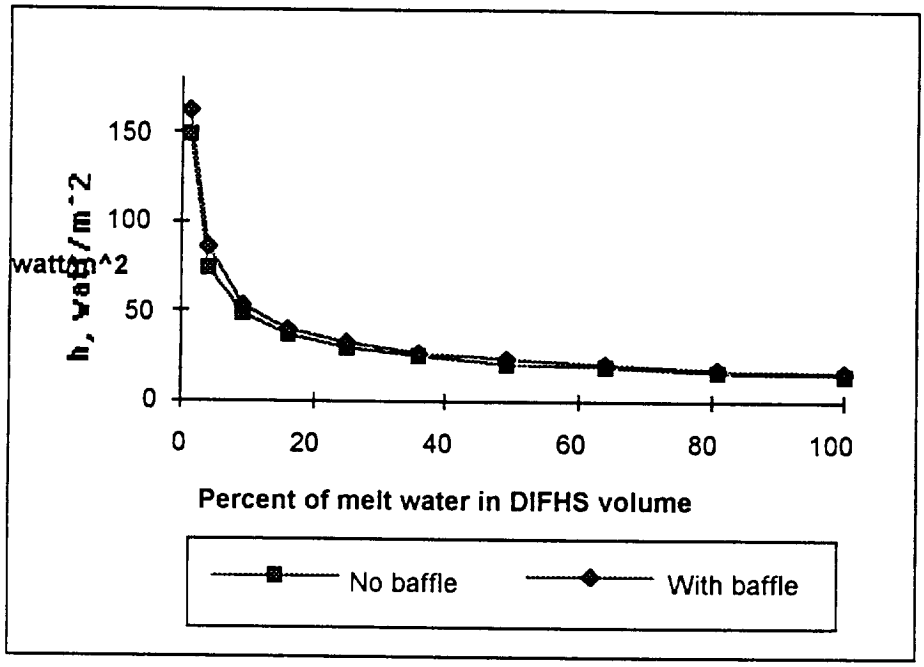

Figure 9. Heat transfer coefficient for laminar flow forced convection

$$\overline{Nu_D} = 3.656 + \frac{K_1\left[D/L \,\mathrm{Re}_D \,\mathrm{Pr}\right]}{1 + K_2\left[D/L \,\mathrm{Re}_D \,\mathrm{Pr}\right]} \qquad [2]$$

In Figure 9, the heat transfer coefficients for laminar flow forced convection are graphed for a non-baffled and baffled DIFHS. The heat transfer lengths were normalized to equivalent volumes of ice and melt water. Although the effects of adding a baffle added only about 9% to the overall heat transfer coefficient in this example, there is a positive result to manipulating the fluid stream.

Interlaced materials

The use of an interlaced material to aid in heat flow in the DIFHS was first proposed in the work by Lomax and Kader. (Ref. 8) They suggested the use of an expanded aluminum foam to reduce the time required for regeneration of the melt water. It was hypothesized that the relatively high thermal conductivity of the interlacing material would improve the transport of heat from the center of the melt water to the outside of the container where it would be convected away by the freezer system. The use of an interlaced material would also be used to increase the heat transfer properties of the LCG water in the DIFHS during use.

In the same fashion as the addition of baffles, it can be shown that an interlaced material may also improve the heat transfer coefficient of the fluid stream in DIFHS. As a first approximation, the interlaced material can be modeled as a bank of staggered tubes lying perpendicular to the fluid flow. The average heat transfer coefficient is estimated by Grimson (Ref. 19) and is presented in Equation [3] as

$$\bar{h} = \frac{k_f}{D} C_1 (\mathrm{Re}_{max})^n \qquad [3]$$

where $\mathrm{Re}_{max} = \dfrac{V_z a}{(a - D)} \Big/ \nu_f$.

Applying this equation to a DIFHS with a maximum LCG mass flow of 240 lb/hr, and with an interlaced material with tendril diameter of D=1mm and pore window width of a=4mm results in predicted heat transfer rates over 12 times greater than without an interlaced material. The graph of predicted heat transfer coefficients vs. a normalized volume of melt water is shown in Figure 10.

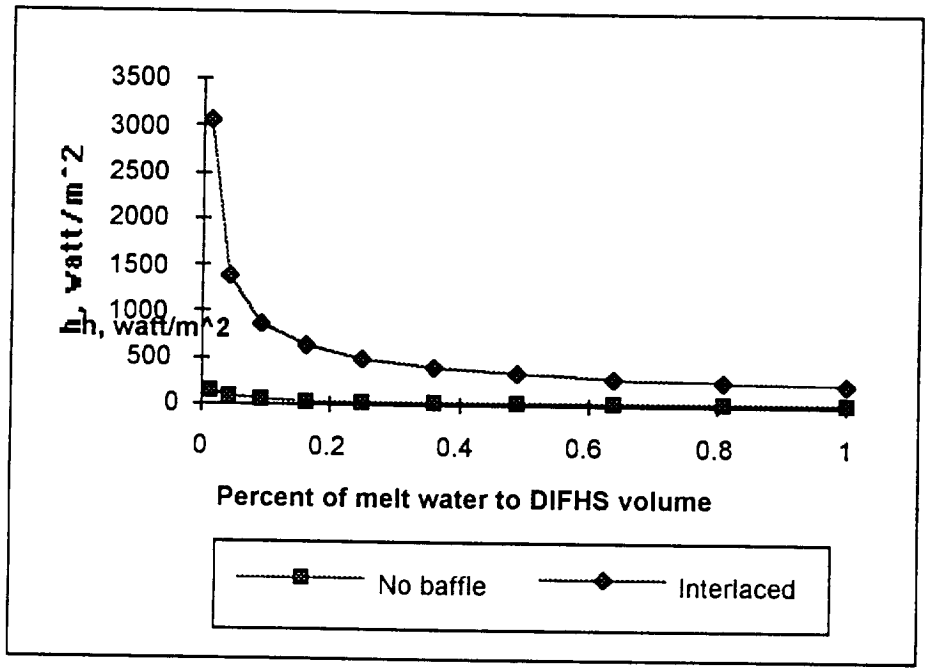

Figure 10. Heat transfer coefficients using an interlaced material of 135W/mK.

The addition of an interlaced material into the DIFHS fluid stream would greatly increase the heat transfer over using no additional material or baffles during use. An interlaced material may provide a practical solution to the inconsistent cooling rates encountered in previous DIFHS prototype testing.

Time to freeze

The use of an interlaced material may decrease the regeneration time for the DIFHS. In a microgravity environment, heat transfer through the melt water is by conduction or forced convection only, due to the lack of natural convection. Natural convection is the physical movement of fluid caused by

buoyant forces arising from density changes. The effects of buoyant forces, that is, forces due to gravity, are negligible in a microgravity environment. (Ref. 6)

The time required for regeneration of the DIFHS can be separated into three distinct processes. First the warm melt water is cooled to the phase transformation temperature. Second, the phase transformation from water to ice occurs, and third, the ice is cooled further to the DIFHS start temperature. As a first approximation for the regeneration time, these three processes can be considered independent which leads to Equation [4]

$$t_{regeneration} = t_{cool\,water} + t_{phase\ transformation} + t_{cool\,ice} \qquad [4]$$

Using a lumped thermal capacity approach to determine the time for each process, the resulting equations are

$$t_{cool\,water} = \frac{T_i - 32}{T_i - T_{freezer}} c_p^{H_2O} \rho_{H_2O} \left[\frac{r^2}{2} \left(\frac{1}{2k_w} + \frac{\ln\left(\frac{r_o}{r}\right)}{k_a} \right) \right]$$

$$t_{phase\,transformation} = \frac{-h_f \rho_{H_2O}}{32 - T_{freezer}} \left[\frac{r^2}{2} \left(\frac{1}{2k_i} + \frac{\ln\left(\frac{r_o}{r}\right)}{k_a} \right) \right]$$

$$t_{cool\,ice} = \frac{32 - T_{end}}{32 - T_{freezer}} c_p^{ice} \rho_{ice} \left[\frac{r^2}{2} \left(\frac{1}{2k_i} + \frac{\ln\left(\frac{r_o}{r}\right)}{k_a} \right) \right]$$

where T_i is the initial melt water temperature, T_{end} is the final temperature of the ice, $T_{freezer}$ is the temperature of the freezer, and r and r_o are the inner and outer radii of the container, respectively.

Assuming an initial melt water temperature of 4.4 °C (40 °F), a final temperature of -17.8 °C (0°F), and a freezer temperature of -23.8 °C (-6 °F) this equation predicts a regeneration time of 17.8 hours for a 0.32 m (12.5 inch)

diameter cylinder. This compares favorably to the regeneration time of 17 hours reported by Lomax and Kader for their 1/2 capacity DIFHS unit. (Ref. 8)

From the above equations, economies in the regeneration time can be realized from the use of lower freezer temperatures, decreased radii for the DIFHS container, and increased thermal conductivities for the fluid and/or the solid phases.

Lower freezer temperatures can reduce the time to freeze for the DIFHS unit, however, reduced temperatures can be directly related to higher heat loads. For radiator freezers, reduced freezer temperatures create higher heat rejection loads which in turn require increased radiator areas to expel the heat into space. Refrigeration systems operating at a greater ΔT require increased power to reject these higher heat loads. (Ref. 6)

Decreasing the total conduction distance in the DIFHS has the cost of increasing the mass of the container. Given a constant total heat load that the DIFHS must absorb, the fusible material volume of the DIFHS remains constant. Deviations from a spherical container, which has the minimum surface area to volume ratio, increases the mass of the container. Changing the container shape from spherical will probably be necessary to fit the unit into the EMU backpack while simultaneously improving the regeneration time.

Increasing the thermal conductivity of the liquid and solid phases will reduce the regeneration time by increasing the heat transfer capabilities within the system.

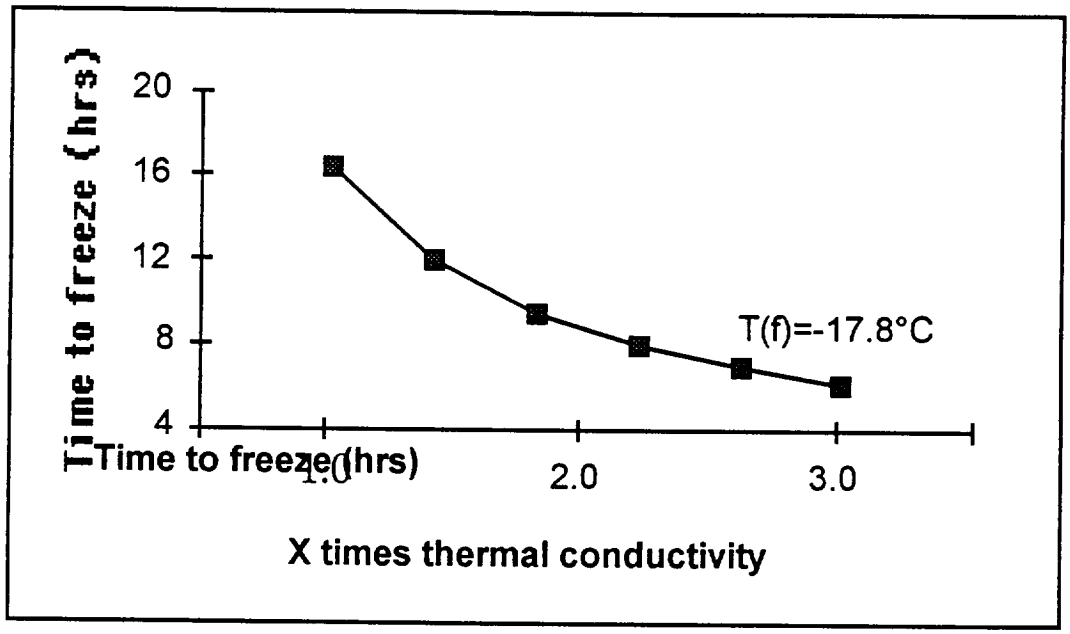

Figure 11. Plot of the time to freeze as a function of effective thermal conductivity

The effect of increased effective thermal conductivities for both the liquid and solid phases on the regeneration time is shown in the graph in Figure 11. The time required for regeneration is plotted against the increased effective thermal conductivity. In this model, it is assumed that the increases in the conductivity values of the liquid and solid phases are proportional. This assumption will be shown to be a valid approximation in the next section.

The addition of an interlacing material inside the Fusible Heat Sink could be used to increase the heat transfer properties of the warm fluid stream to the ice block during use and to increase the relative, or effective, thermal conductivity of both the melt water and the forming ice mass during regeneration. The use of an interlaced material may be advantageous over

baffles because the volume of ice that the fluid must melt through during the start-up condition would be shorter. Additionally, the stresses induced on the tendrils of the interlaced material as the fluid freezes may be less severe than on fixed baffles.

Duocel Aluminum Foam Metal

Prior to this study, a search for potential interlaced materials was performed. (Ref. 8) Interlaced materials are available in a variety of metals including aluminum, nickel, silver, and copper. Other materials are such as silicon carbide, (Ref. 20) vitreous carbon (Ref. 21), and cordierite (Ref. 22) are also available but are typically considered thermal insulators. These interlaced materials have material properties typical of their parent materials. (Ref. 20)

A candidate interlaced material is Duocel Aluminum Foam Metal. It is a proprietary product of the ERG Materials and Aerospace Corporation, of Oakland, CA. A photo of this material is shown in Figure 12. Formed of 6061-T0 aluminum alloy, it has an open-celled structure. The material can be characterized as a skeletal structure of continuous solid metal ligaments forming a matrix of cell-like voids spaces of nominally uniform shape. The void space is a tetrakaidecahedral structure which approximates the equiaxed grain structure in a solid material. The density, strength, and thermal conductivity are all typical of the parent 6061 alloy material. (Ref. 23)

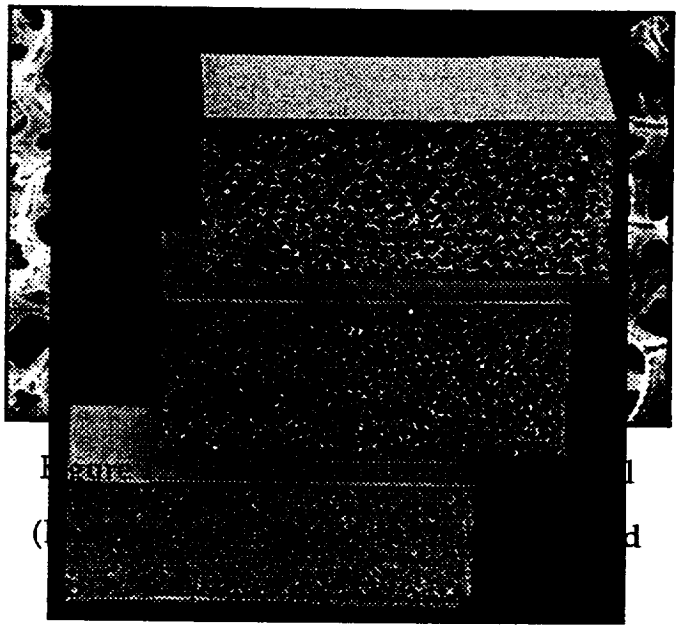

Figure 13. Aluminum foam specimens with equal volume fraction (8%) but different pore sizes (Photo courtesy of NASA-Ames Advanced Life Support Branch)

According to the producer, Duocel is manufactured in a range of pore sizes and volume fractions, from 5 to 40 pores per inch and 3 to 12 percent by volume, respectively. A selection of different pore sizes, each with a relative volume fraction of 8% is shown in Figure 13. Pore size and relative volume fraction are independently variable within a range of values. (Ref. 23)

Duocel represents a candidate of interlaced material that can overcome some of the performance issues of the Direct Interface Fusible Heat Sink. Inefficiencies in heat transfer due to coring, channeling, inefficient mixing, and long regeneration times may be reduced or even eliminated. It fulfills

the high strength, low density, high void fraction, and open pore configuration required for an ideal interlacing material. Its thermal conductivity value is that of the parent material, approximately 135 Watts/mK. The ability to specify both the pore size and volume fraction to optimize the material for use in the DIFHS makes it an attractive candidate.

Thermal conductivity of the aluminum foam

The effect of the interlaced material on the time-to-freeze was a primary factor in the selection process. The thermal conductivities of 6061 aluminum alloy and water are 135 Watt/m-K and 0.607 Watt/m-K, respectively. (Ref. 24) Therefore, the heat transfer properties of the aluminum in concert with the DIFHS water may be utilized to enhance the thermal conductivity of the system.

Overview of effective thermal conductivity models

The effective thermal conductivity of a multi-phase system is a function of the total heat transfer of the system. In theory, the effective thermal conductivity is the summation of all the various paths of heat transfer across and between each of the phases. In practice, models have been developed that use a set of measurable system parameters to predict the overall heat transfer. This section examines a selection of models to determine whether a model may be useful in predicting the effective thermal conductivity of the aluminum foam and water system.

A search of the published literature resulted in ten models being presented here. Each predicts the effective thermal conductivity of a two phase system based either exclusively or primarily on volume fraction the phases. The models presented here are divided into four groups. First, the

bounding equations for effective heat flow are reviewed. Second, models which are based on a system of volume averaging are examined. In the third group, structure-based models are presented, and fourth, models which include additional terms for heat transfer via convection and radiation are reviewed. Excellent reviews of the existing literature are presented by Woodside & Messmer (1961) (Ref. 11) and Collinshaw & Evans (1994). (Ref. 12)

Boundary equations

The absolute upper and lower bounding equations for a two-phase system can be set by using the volumetric law of mixtures. Weighted averages of the conductivities and resistivities of the constituent phases produce the absolute upper and lower bound equations, respectively. These bounding equations are presented as the arithmetic and harmonic models. (Ref. 11, 12)

The arithmetic mean equation mimics the volumetric law of mixtures for parallel streams. This represents an upper bounding equation for heat flow in two phases. As shown in Equation [5], it equates the effective thermal conductivity as the sum of the weighted averages of the phase conductivities.

$$k_{eff} = \varepsilon_f k_f + (1 - \varepsilon_f) k_s \qquad [5]$$

The arithmetic mean model is continuous; that is, as ε_f approaches 0, k_{eff} approaches k_s.. The model implicitly assumes one or more structures for each phase parallel to the direction of heat flow with no interaction between the phases.

The harmonic mean model represents the lower bound of effective conductivity. The harmonic mean assumes heat flow through independent phases located in series. It is mathematically represented as the weighted average of the resistivities of the phases and is presented here as Equation [6].

$$k_{eff} = \frac{k_s k_f}{\varepsilon_f k_f + (1-\varepsilon_f) k_s} \qquad [6]$$

In the same fashion as the arithmetic model, the harmonic mean model is continuous and assumes no interaction between phases. In practice, the effective conductivity is biased towards the lesser conductive material.

Maxwell, in his treatise on electrical conductivity in 1861, developed bounding equations for two special cases of combined phase materials. Although these equations were originally developed for electrical conductivity, they are equally valid for thermal flows. (Ref. 11, 12, 25, 26)

Maxwell's upper bound equation examined a solid matrix containing a suspension of spherical fluid-filled voids or closed pores. It was assumed that the pore volume was small and at the limit, as $(1-\varepsilon_f) \rightarrow 1$, Maxwell's upper equation approaches Equation [7].

$$k_{eff} = k_f \left[\frac{2\frac{k_s}{k_f}(1-\varepsilon_f) + (1-2\varepsilon_f)\frac{k_s}{k_f}}{(1-2\varepsilon_f)\frac{k_s}{k_f} + (1-\varepsilon_f)} \right] \qquad [7]$$

Maxwell's lower bound equation is presented as Equation [8]. Here Maxwell assumes a random distribution of solid spheres in a continuous medium.

$$k_{eff} = k_f \left[\frac{2\varepsilon_f k_f + (3 - 2\varepsilon_f) k_s}{(3 - \varepsilon_f) k_f + \varepsilon_f k_s} \right] \quad \text{where } \varepsilon_f \text{ is large} \quad [8]$$

Because of Maxwell's assumption that the spheres do not interact with each other Equation [8] is limited to when ε_f is large.

Maxwell's bounding equations are based on the assumption that the secondary phase of pores or particles are discrete and therefore non-interacting with other pores/particles. This assumption limits the porosity range although no parameter for limiting the relative size of the pores in given in Maxwell's equation. (Ref. 11, 25) Comparing the Maxwell equations to the arithmetic and harmonic models we observe that due to the assumption of non-interaction of the disperse voids and particles these equations are more limiting.

These equations for maximum and minimum thermal conductivity are important to the current study in that they explicitly relate volume fraction of the phases and implicitly relate the interaction of the phases to the effective thermal conductivity.

Volume averaging models

For multi-phase systems, the simplest expressions for the effective thermal conductivity are those that rely only on the volume fractions of the constituent phases. In their drive towards simplicity, the effect of structure on the effective thermal conductivity is ignored. Three models, the geometric mean, Asaad's empirical model and one by Hadley for packed metal powders are presented.

The Geometric Mean model is a volume fraction averaging method intermediate of the arithmetic and harmonic models presented earlier. It is based on the weighted logarithms of the individual conductivities. Two variations, by Woodside and Messmer and by Langton and Matthews, have appeared in the literature and are presented here as Equations [9] and [10].

Woodside and Messmer's version of the geometric mean model was developed as the product of the separate thermal conductivity's of each phase raised to the power of its respective volume fraction. (Ref. 11)

$$k_{eff} = k_f^{\varepsilon_f} k_s^{\varepsilon_s} \qquad [9]$$

Langton and Matthews presented the weighted geometric mean in the form of logarithms.

$$\log k_{eff} = \varepsilon_f \log k_f + (1 - \varepsilon_f) \log k_s \qquad [10]$$

The advantage of the geometric mean model is its intermediate value between the arithmetic and harmonic mean models. The geometric mean assumes a linear relationship between the logs of the thermal conductivities of the components. Like the arithmetic and harmonic it is continuous across the full range of porosities. The geometric mean does not consider the geometry of the heterogeneous system, nor does it account for any interaction effects between the individual components.

Asaad, (Ref. 27) in his doctoral thesis at U.C. Berkeley (1955), noted that measured effective thermal conductivities tended to follow the power law of the geometric mean model. He allowed for an empirical factor, c (where c is approximately equal to 1), to be added into the power term of the

geometric model to compensate for deviations from unity. Asaad's empirical equation is presented in Equation [11].

$$\frac{k_{eff}}{k_s} = \left(\frac{k_f}{k_s}\right)^m \quad where\ m = c\varepsilon_f\ and\ c \approx 1 \qquad [11]$$

The value of c is adjusted to fit the experimental results. If c=1, then the equation reverts to the Geometric Mean equation.

Hadley (Ref. 26) applied the technique of volume averaging to produce a series of equations from which the effective thermal conductivity could be calculated. We observe in Equation [12], that it is based on a weighted relationship between two competing routes of heat transfer. One route is conduction through a series of particles in contact with each other (parallel conduction) and the other is series conduction through a suspension of separated particles and a low conducting matrix. This second term is equivalent to Maxwell's upper bounding equation presented previously.

$$k_{eff} = k_f \left[(1-\alpha) \frac{\varepsilon_f f + \frac{k_s}{k_f}(1-\varepsilon_f f)}{1-\varepsilon_f(1-\varepsilon_f f)+\frac{k_s}{k_f}\varepsilon_f(1-\varepsilon_f f)} + \alpha \frac{2\left(\frac{k_s}{k_f}\right)^2(1-\varepsilon_f)+(1+2\varepsilon_f)\frac{k_s}{k_f}}{(2-\varepsilon_f)\frac{k_s}{k_f}+1-\varepsilon_f} \right] \qquad [12]$$

The resulting equation uses two empirical terms to weight the effects of these two modes of heat transfer. Alpha is an empirical factor that balances the first and second terms and can vary from $0<\alpha<1$. The second term, f, represents the propensity of the suspension to operate as if the heat flow was in series, from phase to phase, or in parallel, where the heat flows through each individual material independent of the other materials. (Ref. 26) Both of the empirical terms are determined from experimental data.

The three models presented in this section attempt to trade simplicity in the equation for exactness in the results. The equations are formulated using only the volume fractions of the phases, just as the bounding equations presented previously, but without the implicit restriction of structure, and therefore interaction, between the phases. The models developed by Asaad and Hadley use empirical factors to compensate for this generality.

Structure-based parameter terms

This class of equations adds a parameter to describe the structure of a multi-phase system so that structure is explicitly considered to predict the effective thermal conductivity. Mathematical schemes are used to describe the secondary phase structure more accurately than the spherical shape typically assumed in most of the previous models.

De Vries, (Ref. 11) in 1952, amended Maxwell's lower bound equation, presented previously as Eqn. [13], to accept particles of various shapes. This modification allowed changes to the assumed spherical nature of the particle component. DeVries applied this structure component to the calculation of the effective thermal conductivity of unconsolidated soils. The form of De Vries equation presented as Equation [13] is for a two-phase system with a continuous fluid phase and dispersed solid phase.

$$k_{eff} = \frac{\varepsilon_f k_f + (1-\varepsilon_f) F k_s}{\varepsilon_f + (1-\varepsilon_f) F}$$

$$where\ F = \tfrac{1}{3} \sum_{i}^{3} \left[1 + \left(\frac{k_s}{k_f} - 1 \right) g(*) \right]^{-1} \qquad [13]$$

The g(*) terms represent geometric shape factors where g(x)+g(y)+g(z)=1. The set of g(*) terms: g(x)=g(y)=g(z)=1/3 represents a

sphere. In his original work, De Vries chose g(x)=g(y)=1/8 and g(z)=6/8 which represented an ellipsoidal solid whose major axis was 6 times that of the minor axis. Of course, the implicit assumption of non-interaction between the dispersed phase stated in Maxwell's development continues to hold in De Vries equations.

The Unit Cell Model of Dulnev (1965) (Ref. 28, 29, 30), was adapted for use in porous solid materials by Luikov. In this equation the heterogeneous material was modeled as two intertwined three-dimensional networks (solid-fluid) composed of repeated units. The model assumes that the overall thermal conductivity can be developed by determining the conductivity of an elementary volume, or unit cell, whose edges create a skeletal framework that approximates the continuous phase. The non-continuous phase is the resulting volume remaining.

Luikov allowed for four independent modes of heat transfer; conduction through the solid phase, conduction through the fluid medium, radiative heat transfer between the surfaces, and gas convection within the pores. Additionally, contact resistance between particles may also be accounted for. The Luikov equation for a two component system with interconnected pores (Ref. 28) is presented in Equation [14].

$$k_{eff} = k_s \left[\left(\frac{h}{L}\right)^2 + \frac{k_g'}{k_s}\left(1-\left(\frac{h}{L}\right)\right)^2 + \frac{2\frac{k_g'}{k_s}\frac{h}{L}\left(1-\frac{h}{L}\right)}{1-\frac{h}{L}+\frac{k_g'}{k_s}\frac{h}{L}} \right] \qquad [14]$$

where $k_g' = k_{g\,conduction} + k_{g\,radiation}$

The Dulnev/Luikov model has the capability of explicitly modeling dual continuous systems such as the aluminum foam and water system considered in this study. The pore geometry, thermal conductivities and volume fractions of the individual components are explicitly input. The addition of a characteristic pore length, L, however, allows the model to compensate for deviations from strict one-dimensional flow that this modeling scheme relies. That is, the characteristic length is calculated from empirical data so that the model agrees with experimentally determined results.

The structure-based models explicitly consider the interaction between the phases in predicting the effective thermal conductivity. These models require more information about the system than the volume averaging equations presented earlier which may or may not increase the accuracy of the prediction. The use of empirical coefficients in some of the volume averaging models and the use of a characteristic pore length in the Luikov/Dulnev model allow the models to correlate to the experimental results which may be influenced by other factors.

Contact resistance and other additional terms

Additional modes of heat transfer such as contact resistance, convection, and radiation may influence the thermal conductivity. Contact resistance can impede, or decrease, the heat transfer between particles or phases. As observed in the previous model by Dulnev, the effect of contact resistance between particles can be explicitly accounted for. Heat flow via convection and/or radiation within the pores increases the thermal conductivity. (Ref. 19, 22) In practice the effects of convection and radiation decrease as the pore size and mean temperature decrease, respectively.

Convection is considered negligible at pore diameters less than 6-10 mm or when the Grashof-Prandtl number (Gr. Pr) is less than 10^3. (Ref. 12, 19, 31) Similarly, the effects of radiation are considered negligible at temperatures less than 600°K. (Ref. 12, 19)

The inclusion of additional transfer terms such as radiation, convection, and contact resistance are usually simplified as being additive. That is, the effective conductivity is the sum of the separate terms.

$$k_{eff} = k_{conduction} + k_{radiation} + k_{convection} + k_{contact}$$

While the assumption of additive paths allows convenient simplicity it can also detract from exactness. (Ref. 11)

A model developed for ceramic foams with interconnected pores was developed by Zumbrunnen, Viskanta, and Incopera, (Ref. 22) and is presented as Equation [15]. This model considers many of the same parameters as the Dulnev/Luikov model. It assumes an elementary set of pathways for heat transfer within the material. For example, a set of pathways could be: heat flow across a particle, through the matrix phase, and through the matrix and then across a particle. The total thermal conductivity then is the sum of the heat flows across these pathways weighted by the probability of their occurrence.

$$k_{eff} = \left[\zeta + \Lambda\left(\frac{\beta+1}{\beta}\right) + 1\right]\left[\frac{1}{\lambda_s}\left(\frac{\Lambda\psi}{\beta} + \zeta\right) + (1+\Lambda)\left(\nu h_{rv} + \frac{k_f}{\varphi}\right)^{-1}\right]^{-1} \quad [15]$$

Where $\beta = \dfrac{\varphi^{1/3}}{1-\varphi^{1/3}}$

$\psi = 0$ *for open pore systems*

$= 1$ *for closed pore systems*

$$vh_{rv} = \text{radiation contribution term}$$

$$\varphi = \text{characteristic pore ratio} = \frac{\text{effective length for conduction in pore}}{\text{characteristic size of pores in solid}}$$

$$\Lambda = 1 + \ln\left(\frac{\beta+1}{\beta}\right)^{-1}$$

and

$$\zeta = \frac{(1+\beta)\left(\frac{2+\beta}{1+\beta}\right)\ln(1+\beta)+1}{\beta\ln(1+\beta)}$$

The Zumbrunnen model assumes that convection within a pore is negligible but defines conduction across a pore as a ratio proportional to the effective length for conduction across a pore to the characteristic pore length. Therefore, in practice the effects of convection may be considered. The model allows for conduction through two continuous phases (parallel conduction).

Model comparison

In order to visualize the range of predictions for the effective thermal conductivity that these ten models generate, a hypothetical two phase system was analyzed. The system was assumed to be equivalent in structure to the aluminum foam and water systems considered in this study. Both phases were continuous through the bulk with the low conductivity phase having the greater volume fraction. The phases were assigned conductivities of 0.6 and 135 W/mK, respectively. Structure parameters required for some models are given with the tabular data.

For the range of volume fractions from 0 to 10% for the high conductivity material the effective thermal conductivities predicted by the

Table 3. Effective thermal conductivities predicted by ten models

ten models are presented in tabular and graphical form in Table 3 and Figure 14, respectively.

%Volume Fraction, Foam	3.7%	3.8%	5.2%	5.6%	6.0%	6.1%	7.7%
Arithmetic	5.62	5.79	7.67	8.23	8.85	8.92	11.04
Harmonic	0.63	0.63	0.64	0.65	0.65	0.65	0.66
Upper Maxwell	4.00	4.12	5.41	5.80	6.23	6.27	7.76
Lower Maxwell	0.68	0.68	0.71	0.72	0.73	0.73	0.76
Geometric	0.74	0.75	0.81	0.82	0.85	0.85	0.92
de Vries	1.13	1.15	1.35	1.41	1.48	1.49	1.73
Asaad	1.32	1.33	1.42	1.45	1.48	1.48	1.60
Dulnev	1.24	3.29	2.09	1.69	2.13	1.42	0.78
Zumbrennen, et al	1.47	1.47	1.48	1.49	1.49	1.49	1.50
Hadley	1.16	1.18	1.36	1.42	1.48	1.49	1.69

From the table and graph it can be observed that each of the models lie between the arithmetic (upper bounding) and harmonic mean (lower bounding) models which was expected. The models generally predict a conservative effective thermal conductivity.

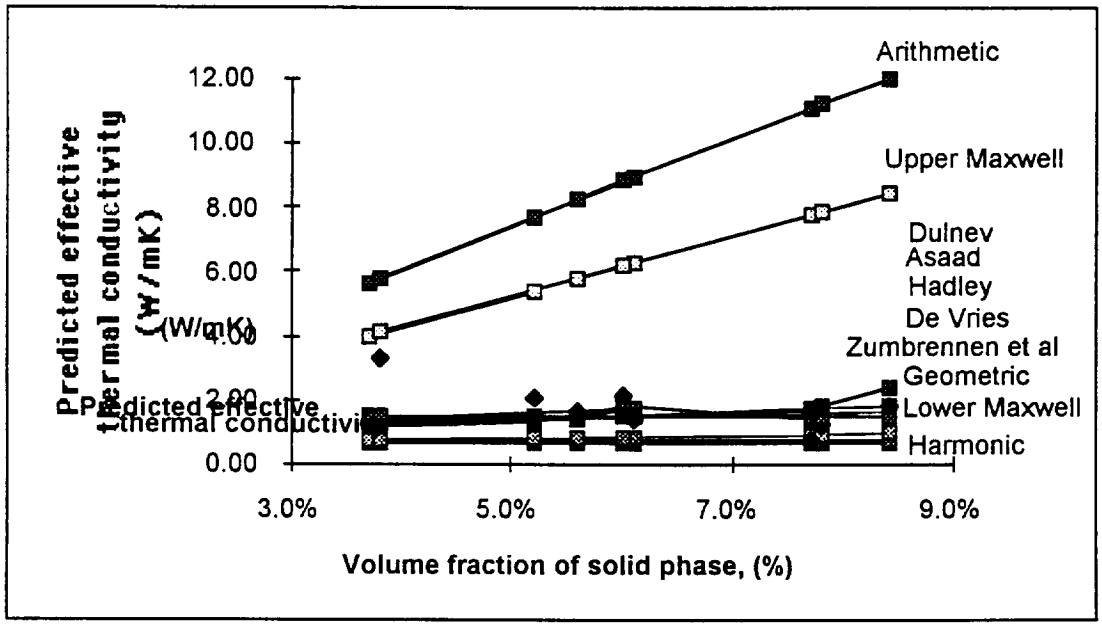

Figure 14. Plot of model predictions of effective thermal conductivity as a function of interlaced volume fraction

Experimental method development

Due to the wide spread of effective conductivities that the empirical models predicted, the next step was to experimentally determine the effective

thermal conductivity. A literature review was conducted to obtain an overview of the methods used to measure thermal conductivity. Additionally, a number of independent testing labs, testing equipment distributors, and equipment producers were interviewed to determine whether any testing method had a practical advantage over the other methods.

From the literature review, a number of different methods to measure the effective thermal conductivity were found. In general, they can be separated into two classes; steady state and transient. Steady state methods rely on an equilibrium state of heat flow. The thermal conductivity is then solved directly utilizing Fourier's law. Steady state methods are computationally simpler to extract the thermal conductivity but heat leaks out of the system make practical measurements difficult.

Transient methods, in general, relate the temperature change over time of a known sensor/heat source in contact with the test material to the thermal properties of the material itself. Transient methods have the advantage of not having to achieve and maintain an equilibrium state of heat flow. The disadvantages of transient systems include the inability to test across a large volume; most transient methods minimize the test surface to a line or point. This deficiency increases possible error where the measured heat conductance over the test distance may not be representative of the thermal conductivity.

Interviews with engineers and salespeople associated with testing labs, test equipment distributors, and producers revealed no consistent method for determining thermal conductivity. Of the nearly one dozen

companies that were contacted, only one method, the Guarded Heat Stack (ASTM E1225) was offered by more than one respondent.

Table 4 lists a selection of methods taken from the literature and from recommendations by thermal engineers that can be used to determine thermal conductivity. Some methods are applicable only to solids or to insulative materials, while others are very general in theory. Oftentimes, the experimental apparatus must be optimized to the range of conductivities expected from the test material.

Table 4. Summary of methods to measure the effective thermal conductivity

Method		Description
ASTM 2717-90 (Ref. 32)	Steady State	The 4-lead platinum heat source in a thin glass tube. Known energy input, temperature gradient is measured. Small conduction distance (gap) required to prevent convection. Non-metallic liquids only. Precision reported to 10%
ASTM E-1225-87 Guarded Stack (Comparator) (Ref. 33, 34, 35)	Steady state	Specimen is sandwiched between two reference materials. ÆT between reference blocks is measured. Heated guards and insulation are utilized to minimize heat losses through sides. Relative method. Solids. Precision reported to 6.8% (300K<T<600K)
Unguarded Stack (Ref. 36)	Steady State	A variation of Guarded Stack Method (ASTM 1225-87) without the use of guards. Larger error possible. Insulative materials only.
Concentric Spheres (Ref. 37)	Steady state	Heater in central sphere, sample in gap between spheres. Realizes theoretical conditions of no heat loss without the use of guard heaters. Liquids, solid-liquid composites (microbeads) and powdered solids.
Transient Hot Strip (THS) (Ref. 38, 39, 40)	Transient	Constant power planar heat source. Change in resistance across heater related to q. Resistance across heater measured. Low temperature increase (1 degree K). Powdered metals, liquids and solids of low thermal conductivity. Precision reported to within 3%.
Transient Hot Wire (Ref. 41, 42, 43)	Transient	Constant power radial heat source. Assumes the relation of temperature vs. ln(time) is linear and the slope contains the TC of the material the wire is pressed against. Insensitive to plastic flow. Good contact is required to attain true readings. Precision to within 2% of reported standards. Solids and liquids under pressure.
Longitudinal Test with Profiled Guard (Ref. 43, 44)	Steady state	This method uses a close fitting guard around a cylindrical sample plus a second outer guard at the heat sink temperature. Solids and powdered samples
Horizontal Flat plate (Ref. 45)	Steady State	Thin fluid film between two metal plates. Heated guard plate required. Convection can be suppressed by decreasing the thickness of the fluid film. Flat plate method is only optimal for fluids at their critical point with gap widths of a few hundredths of a millimeter. Fluids.
Kohlrausch Heat Conductivity (Ref. 46)	Steady State	Constant electrical current is passed through material. Joule heating creates thermal gradient along bar. Thermal conductivity is determined from electrical conductivity measured.

Requirements for the experimental method

The measurement of the effective thermal conductivity of the foam + water system is difficult due to the complex nature of the system. In general, any applicable method must consider the conditions imposed by the material to be tested. The appropriate experimental method must have the ability to measure a liquid and solid composite material. The presence of a liquid phase raises the possibility of convective heat transfer during the testing period. Heat transfer sue to the onset of convection within the pores may or may not be significant to the overall conductivity of the system. The typical solution to avoid convection is to reduce the conduction distance to a minimum. The aluminum foam, on the other hand, restricts the minimum conduction distance. Since the pore size is fixed the conduction distance must be at least that of the pore diameter. More appropriately, the distance should be much greater than the pore diameter because of inhomogeneous pore size distribution throughout the foam.

For steady state methods, where a temperature gradient is used, additional test constraints apply. The absolute temperature range of the system is between 0°C and 100°C. The largest temperature gradient possible across the system will be less than 100° Celsius. It is possible to maintain a larger gradient across the test fixture where reference materials are stacked above and/or below the specimen but the gradient through the specimen must not exceed 100°C.

For transient testing where a heat front is applied to the system the penetration of that heat front must at least exceed the maximum pore size of the aluminum foam test specimens. The maximum pore size of the aluminum foam specimens to be tested is approximately 5mm.

Of the various measurement techniques listed in Table 4, the three most likely candidate methods to determine the effective thermal conductivity of the foam + water system in this study are the Guarded Heat Stack (ASTM E1225), Hot Wire (ASTM C1113), and the Transient Hot Strip techniques.

Guarded Heat Stack ASTM E-1225-87

The Guarded Heat Stack method (Ref. 33, 34, 35) is the primary ASTM standard method for measuring the thermal conductivity of solid materials. In theory, a one-dimensional heat flow is established in the test material. The thermal conductivity is then measured directly using Fourier's equation for steady state heat flow

$$k = -q\frac{\Delta Z}{\Delta T} \qquad [16]$$

where ΔZ is the thickness of the material in the heat flow direction. The heat flow, q, is determined by the use a reference material in-line with the test sample.

In practice, the test specimen is placed in a vertical stack between two reference materials. Heat is supplied from above from a heater; heat flow, q, is determined by temperature readings above and below each reference block. The temperature gradient across the test specimen determines the thermal conductivity. Heated guards and insulation along the sides are utilized to minimize heat losses through the sides of the reference blocks and test specimen.

The difficulty encountered with the Guarded Heat Stack is the establishment of one-dimensional heat flow. (Ref. 33) Heater guards and

insulation are required to maintain this condition. To compensate for heat losses through the sides the thermal conductivity of the insulation between stacks and guards must be known. A heat shunting equation is provided in the ASTM write-up to calculate these heat losses. Reference materials of equal or slightly greater thermal conductivity as the test specimen aid in establishing linear heat flows. Precision is reported by the ASTM to be within 6.8% within the temperature range of 300°K to 600°K (80°-620°F).

With respect to the system at hand the Guarded Heat Stack offers an easy test equipment set-up, however the temperature differential across the test material limits its applicability. The absolute temperatures of the foam + water system are 0° and 100°C (32° and 212°F) due to phase transitions. This allows a maximum differential of 100°C. This range also is just outside the recommended temperature, which may reduce accuracy. Additionally, convection may occur during testing due to the temperature differential which would introduce inaccuracies into the results.

Hot Wire, ASTM C 1113-90 (Platinum Resistance Thermometer Technique)

The Hot Wire method (Ref. 41, 42, 43) was developed to measure the thermal conductivity of non-carbonaceous, dielectric refractories. The method uses a platinum wire as a heat source and resistance thermometer. A constant current electrical load through the wire causes Joule heating to occur which in turn heats the surrounding sample material. By measuring the temperature increase and the power input to the wire the thermal conductivity can be calculated by using the time dependent Fourier equation for heat flow from a line source

$$k = \frac{qd\ln(t)}{4\pi dT} \qquad [17]$$

The method is specified for dielectric materials under 15 watt/mK within a temperature range of room temperature to 1500°C (2700°F). Only small changes in the bulk temperature occur during testing, reported to be approximately 1°C (2°F). The time to test is approximately 10 minutes. (Ref. 41, 42)

The Hot Wire method is limited to dielectric materials due to the use of a bare metal lead (platinum) as the heat source. However, this constraint may be circumvented by the use of an electrically insulating paint over the wire for use with the electrically conductive foam + water system. (Ref. 42)

The Hot Wire method is limited by the use of a line source as the heating element. The effective test volume may be less than the pore size of the foam material. The measurement of anisotropic materials, and especially those containing fibers, are not recommended using this method. (Ref. 43)

Transient Hot Strip (THS)

The Transient Hot Strip method (Ref. 38, 39, 40) is similar in theory to the Hot Wire method but uses an extended metal strip (at least a 20:1 length to width ratio) as a planar source of heat and temperature sensor. As in the previous method, a constant voltage is passed through the strip but here the change in resistance of the strip over time is recorded. The relationship between the resistance and time is given as Equation [18]

$$R = R_o + Cf(\tau_c) \qquad [18]$$

where the time is represented by a function of τ for the material. The slope of this function is proportional to the thermal conductivity where

$$k = \frac{\alpha R_0 I_0^2}{2\sqrt{\pi h C}} \qquad [19]$$

This method for measuring thermal conductivity has been cited in numerous recent papers for a wide variation of materials and conductivities. For example, powdered metals, (Ref. 47) liquids, (Ref. 39) and solids of low thermal conductivity (Ref. 38, 39, 48) have been measured using this method. Parameters attractive to this study include low increase in the bulk temperature(Å1° K) and a short test time interval (<1 minute). Electrically conductive materials have been tested with this method using an insulating layer between the strip and material. (Ref. 40) Accuracy was reported by the original authors to be within 3%. (Ref. 39)

The Transient Hot Strip method has specific advantages over the other two candidate methods in determining the effective thermal conductivity of a foam+water system. The low bulk temperature increase, which will minimize convection, is a clear advantage over the Guarded Heat Stack method. In comparison to the Hot Wire method, the volume of analysis using the THS method is greater due to greater power inputs and the increased surface area of the heat source. This may increase the repeatability of the analysis for an anisotropic material. The analysis time period is shorter, though, on the order of one minute versus ten minutes for the Hot Wire method. A shorter analysis time may increase error due to the heat capacity of the insulating cover required for electrically conductive samples.

Alternatives to the sublimator system for cooling astronauts during EVA have been presented. The Direct Interface Fusible Heat Sink (DIFHS) is a viable option for use in an ISS EMU provided the regeneration time between sorties can be reduced. The use of an interlaced aluminum foam in

the DIFHS water to increase the effective thermal conductivity may provide that reduction in time. A review of the literature revealed that models to predict the effective thermal conductivity may vary over an order of magnitude or require experimentally derived coefficients. Experimental methods to determine the effective conductivity were reviewed. The Transient Hot Strip (THS) method was determined to overcome most of the difficulties in measuring this two-phase system.

In the next section the research objective to experimentally measure the effective thermal conductivity will be presented. The sections following the objective statement outline the procedures used and discuss the results of testing.

Research Objective

The primary objective of this investigation was to measure the effective thermal conductivity of an aluminum foam + water system. It was hypothesized that the effective thermal conductivity is both a function of the volume fractions of the individual components in the system and their structure. The contribution of both the volume fraction and pore size to the effective thermal conductivity was determined. The results of the experiment was compared to a selection of published equations that each predict the effective thermal conductivity for multi-phase systems.

Experimental procedure

In the previous sections, a case for the Direct Interface Fusible Heat Sink as a viable alternative to the sublimator for astronaut cooling during EVA has been presented. A disadvantage in the DIFHS is the regeneration time needed to refreeze the unit between sorties. A solution to reduce this time is the use of an interlaced aluminum foam to increase the effective thermal conductivity. However, equations to predict the effective conductivity vary over an order of magnitude and/or require empirical coefficients which require experimental measurements to determine.

To measure the effective thermal conductivity the Transient Hot Strip method was used. In this section the unique considerations of the foam+water system are presented and the design of the test system is reviewed. Procedures are outlined for establishing system coefficients, obtaining calibration checks, and acquiring and reducing data to determine the effective thermal conductivity of the foam+water samples.

In addition to measuring the effective thermal conductivity, the average pore size and volume fraction of the aluminum foam samples were measured. These procedures are also outlined in this section.

Range of measured thermal conductivity expected

In these experiments the range of expected thermal conductivities was from 0.6 to 12.0 W/mK. This range was based on the conductivity of pure water and the conductivity predicted by the arithmetic, or parallel flow model, for a 92% water, 8% aluminum (Al 6061) system.

Equipment design

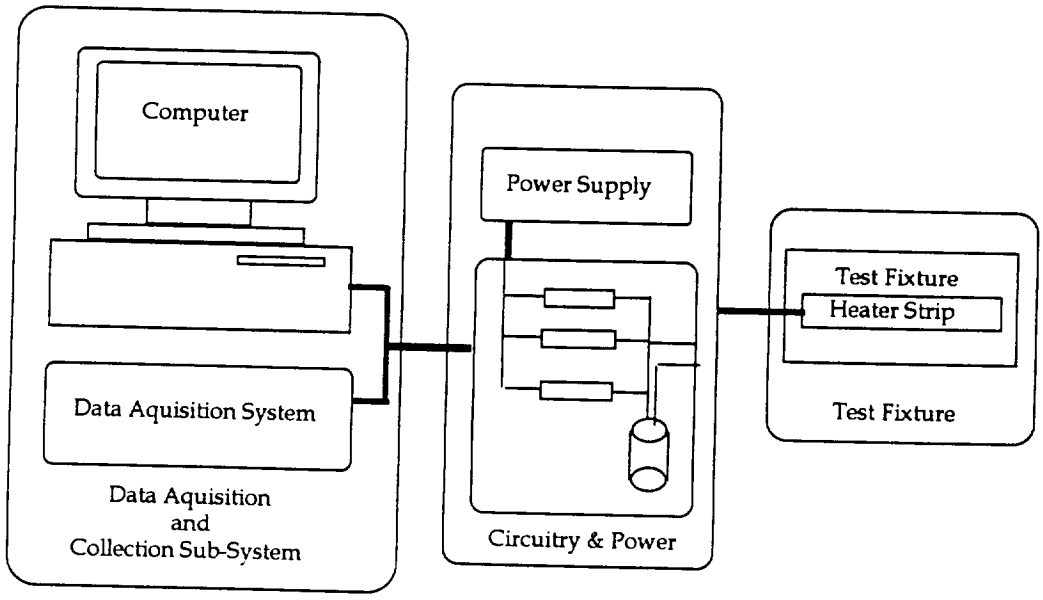

Figure 15. Schematic of equipment sub-systems

The equipment used for this study to determine the effective thermal conductivity of the aluminum foam and water specimens consisted of three separate subsystems; the computer/data acquisition system, controlling circuitry and power supply, and the test fixture which included the heater strip. A schematic of these sub-systems is shown in Figure 15.

Computer and data acquisition equipment

Data collection was controlled by a Macintosh IIfx personal computer using Strawberry Tree data acquisition boards and software. Timers and switch relays were triggered directly by the software. The voltages across the hot strip and the current sensing resistor were logged at a rate of 10 readings per second (10 Hz) at a resolution of 0.000001 V. Temperature readings from the thermocouple were calculated and logged directly by the software.

Control circuit design

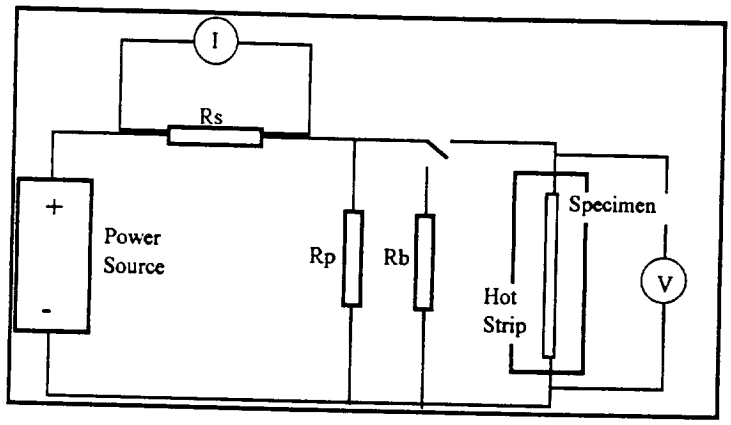

Figure 16. Circuit design for Hot Strip

The electrical circuit for the experiment consisted of a constant voltage power source which fed two parallel circuits. A schematic of the circuit is shown in Figure 16. The primary circuit was made up of the heater strip in series with a time independent resistor, Rs, from which the current for the circuit could be measured. In the secondary circuit, a parallel resistor, Rp, was placed. The resistor, Rp, was used to offset the internal resistance of the power supply.

In order to avoid even a small time dependence in Rs, a balancing circuit with a switch and balance resistor, Rb, was included. The balancing circuit allowed the system to achieve steady state before the test was actually run. The balancing circuit was wired parallel to the heater strip. The circuit was controlled by a relay which allowed current to pass through only Rb prior to and only through the heater strip during the test. The value of Rb was chosen to be very nearly the same as the resistance of the heater strip.

Power source

A Hewlett-Packard E3617A variable power supply was used as a power source for the hot strip circuit. The unit has a maximum output of 50V and 3A. The resistors and relay were soldered directly to a circuit board.

Test Fixture

A fixture to house the foam and water specimen and heater strip during testing was constructed. Made of an acrylic block, a test cell was machined into the block to accept the test specimens and heater strip in a horizontal position. The test cell had inner dimensions of approximately 8.5 x 4.0 x 4.0 cm^3. The outer dimensions were 15.5 x 10.0 x 6.0 cm^3.

Heater strip(s)

The typical set-up for the heater strip/temperature sensor is a metal strip as the electrically-conductive heat source. (Ref. 39) The heat source used in this experiment was a heater element developed by Southwall Technologies. The heater strip was formed from vapor-deposited copper on a Kapton substrate. Electrical leads were soldered to the ends of the formed strip. A second layer of Kapton was then fused to the first to obtain a permanent seal around the metal strip.

The heater leads were silver soldered to longer lead wires which were in turn terminated into a Molex-style plug. This plug allowed different width heater strips to be interchanged dependent upon the expected thermal conductivity. Figure 17 shows a typical heater strip.

The width of the heater strip used for the tests was based on the expected diffusivities that would be encountered and the practical time period required to acquire a sufficient number of measurement points. The practical time span was determined to be about 20-25 seconds. The relationship between the length of the test (characteristic time, θ) and the half-width, d, of the strip is given by Equation [20]

Figure 17. Heater strip

$$\theta = \frac{d^2}{k/\rho C_p} = \frac{d^2 \rho C_p}{k} \qquad [20]$$

where k is the thermal conductivity, ρ is the density, and C_p is the specific heat at constant pressure.

Given a thermal conductivity, density, and specific heat for pure water of 0.6 W/mK, 0.998 g/cm^3, and 4.18 J/gK, respectively the strip width for pure water was determined to be approximately 3.0 mm. Similar calculations for a 92% water, 8% aluminum (Al 6061) system would yield a strip width of 3.5mm.

The requirement for the length of the heater strip is that the ratio of length to width be approximately 20. (Ref. 40) This is to minimize the effects of heat flow along the length (z-direction). Therefore, for these experiments, the strip length must be approximately 70 mm.

The actual dimensions of the strip used for these experiments for foam + water combinations was 7.9 x 0.30 x 0.0025 cm^3.

Determining the TCR of strip(s)

The temperature coefficient of resistivity (TCR) for each strip was determined by measuring resistance at a series of temperatures between 0° and 100°C.

Each strip was tested by connecting the strip to the test apparatus. The strip was then placed in a water bath above a hot plate/magnetic stirrer. The magnetic stirrer allowed the water in the bath to circulate to achieve a uniform temperature. The hot plate was used to maintain the temperature of the bath above room temperatures for additional readings.

A low current, 0.1 to 0.2A, was applied to the strip and its resistance was measured to the nearest 0.000001 Ω. The temperature of the water bath was recorded to within 0.1° with an NIST-traceable thermometer. The resistance and temperature were recorded a minimum of 3 times at each temperature.

The strip was placed in a 0°C ice bath and the resistance and temperature recorded. The ice bath was replaced with a water bath at room temperature and additional temperature and resistance measurements were recorded. The strip and thermometer were then immersed in a boiling water bath where resistance and temperature readings were recorded.

The data were plotted graphically as resistance as a function of temperature. A second order equation was fitted to the data. The temperature coefficient of resistivity was then calculated by Equation [21] where

$$\alpha = \frac{1}{R}\frac{\partial R}{\partial T} \qquad [21]$$

The temperature coefficient of resistivity for the strip was determined to be $4.14 \times 10^{-3}\ C^{-1}$ at 22.0° C which compares with a listed value of 0.0068 /C° for pure copper at 20°C (Ref. 49).

Calibration of equipment

Preliminary tests were made on a standard material in order to determine the accuracy of the test equipment. The reference material chosen was within the range of expected thermal conductivities. The reference materials was pure water. Additionally, testing of a liquid (water) allowed the effects of convection on the test results to be determined.

Procedure for data collection

For this study a matrix of aluminum foam + water specimens were used to determine the effect of pore size on the effective thermal conductivity. The specimens represented three volume fractions crossed with three pore sizes resulting in an array of nine specimens. The pore size, volume fraction, and effective thermal conductivity were determined for each specimen.

Bias was minimized during testing of the foam and water specimens by testing in a round robin sequence. Each specimen was mounted in the fixture, allowed to equilibrate, tested, then removed. Replications for each specimen were done independently.

Mounting of specimens to reduce contact resistance

Specimens were mounted in the chamber so that the strip would lie in a horizontal position with the separate halves of the foam above and below the heater strip. A wedge was used to reduce contact resistance. Figure 18

shows the bottom half of the aluminum foam specimen inserted in the test cell and heater strip positioned.

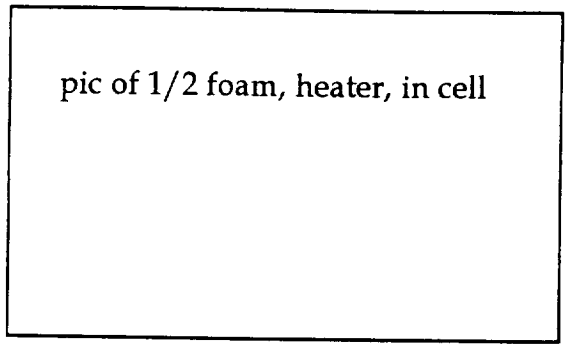

Figure 18. Aluminum foam sample in test fixture

To mount the specimen for testing the test chamber was filled with de-ionized water. The first, or bottom, half of the specimen was placed in the fixture and the entire fixture was tamped against the table top to dislodge any trapped air bubbles that may have been trapped inside the pores of the specimen. The heater strip was laid on top of the specimen. The second half of the foam specimen was then laid on top of the heater strip. Additional water was added to completely fill the test chamber. Additional tamping removed any trapped air bubbles in the second piece of foam. Contact resistance was minimized by compressing the two halves of the foam and the heater strip against the bottom of the chamber while inserting a wooden wedge between the sides of the foam and the chamber wall. A T-type thermocouple was placed into the foam to determine when thermal equilibrium of the test system was achieved and to record the initial temperature.

Equilibrium temperature

Prior to each test the specimen and test fixture was allowed to equilibrate in temperature. A T-type thermocouple was inserted into the specimen prior to testing. Temperature equilibrium was assumed to be

attained when the temperature indicated by the thermocouple fluctuated less than 0.5°C over a 30-second time period.

Recording of data

The collection of data was initiated, controlled, and logged by a data acquisition system run through a desktop computer. Data logged consisted of bulk temperature, elapsed time, voltage generated by the power source, voltage across the heater strip, and voltage across the current sensing resistor. Separate data files were created for each test and saved electronically for later spreadsheet manipulation. A sample of the logged data is shown in graphical form in Figure 19.

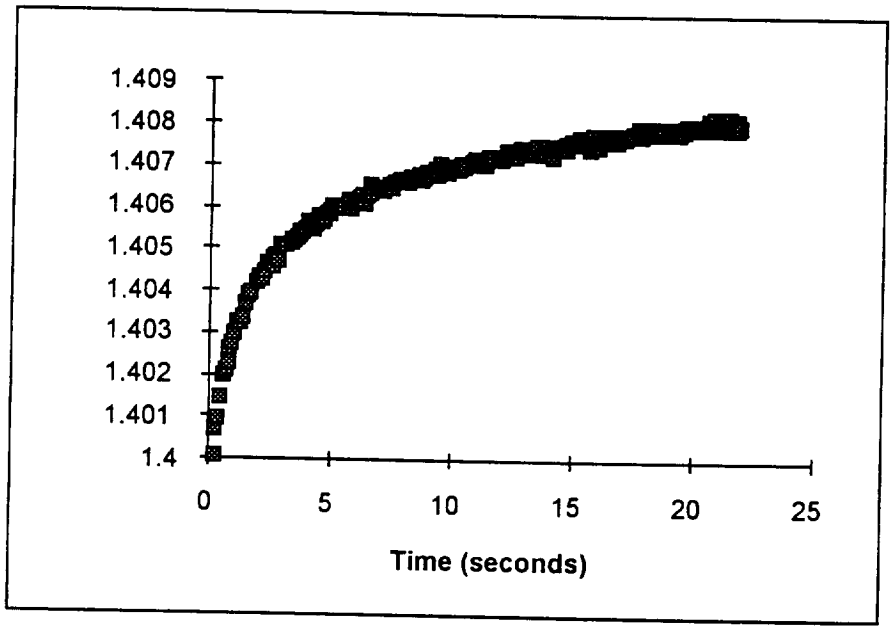

Figure 19. Sample data of resistance versus time.

Calculations to determine the thermal conductivity

Determining the time delay, t_c, of strip(s)

A time delay, t_c, is encountered in the heat flow from the hot strip to the test material due to the electrically-insulating layer surrounding the strip.

According to Gustafsson, Karawacki, and Chohan (1986) (Ref. 40) the time delay due to a thin insulating strip can be expressed by the relationship presented as Equation [22]

$$R = R_* + A(t - t_c)^{1/2} + B(t - t_c) \qquad [22]$$

where A and B are constants.

By plotting resistance versus $(t - t_c)^{1/2}$, a t_c was chosen through an iterative procedure such that the deviations of the experimental measurements to the theoretical curve assumed a minimum value. Additionally, the apparent resistance, R*, as the y-intercept, was extrapolated from this equation.

Determining f(τ)

By plotting the resistance versus the function f(τ). A linear regression of the data will yield an equation of the form

$$R = R_o + Cf(\tau) \qquad [23]$$

where the parameters of the line; C, the slope, and R_o, the y-intercept, are used to determine both the diffusivity and the thermal conductivity.

The function f(τ) is defined as

$$f(\tau) = -erfc\left(1/\tau\right) - \frac{\tau^2}{\sqrt{4\pi}}\left[1 - \exp\left(\frac{-1}{\tau^2}\right)\right] + \frac{1}{\sqrt{4\pi}}\left[-Ei\left(\frac{-1}{\tau^2}\right)\right] \qquad [24]$$

where

$$\tau = \sqrt{\frac{t - t_c}{\theta}}$$

$$erfc(u) = 2(\pi)^{-1/2} \int_u^\infty \exp(-\upsilon^2) d\upsilon$$

$$-Ei(-u) = \int_u^\infty \upsilon^{-1} \exp(-\upsilon) d\upsilon$$

Polynomial approximation of Ei(x)

The mathematical function of -Ei(-u) was approximated by a polynomial function given by Abramowitz and Stegun (Ref. 50) and presented here as Equation [25]

$$-Ei(-x) = E_1(x) \approx \left[\frac{x^4 + a_1 x^3 + a_2 x^2 + a_3 x + a_4}{x^4 + b_1 x^3 + b_2 x^2 + b_3 x + b_4} + \varepsilon(x) \right] \left(x e^x \right)^{-1}$$

$$|\varepsilon(x)| < 2 \times 10^{-8} \qquad [25]$$

$$a_1 = 8.57332\ 87401 \quad b_1 = 9.57332\ 23454$$
$$a_2 = 18.05901\ 69730 \quad b_2 = 25.63295\ 61486$$
$$a_3 = 8.63476\ 08925 \quad b_3 = 21.09965\ 30827$$
$$a_4 = 0.26777\ 37343 \quad b_4 = 3.95849\ 69228$$

Determining the Diffusivity and Thermal conductivity

According to prior work by Gustafsson, Karawacki, and Khan, (Ref. 39) the deviations of the experimental measurements from a linear equation will be minimized when θ, the characteristic time value, is correct. By using an iteration procedure it is possible to determine a θ such that the correlation coefficient achieves a maximum value. The diffusivity can then be determined directly from the relationship

$$\kappa = \frac{d^2}{\theta} \qquad [26]$$

From the equation of the line for the resistance versus f(τ) the thermal conductivity, *k*, was calculated from the relationship

$$k_{eff} = \frac{\alpha R_s R_0 I_0^2}{2\sqrt{\pi} hC} \qquad [27]$$

Procedure for measuring pore size

The pore sizes of the aluminum foam specimens were determined by using the Circular Intercept Method of the ASTM standard E112-88 *Standard Test Methods for Determining Average Grain Size.*. (Ref. 51)

To analyze the foam specimens a two-dimensional representation of each specimen was required. The two large faces of each specimen were pressed into a thin layer of modeling clay approximately 1/8". The impression in the clay layer was photocopied on a Xerox copy machine to enhance the contrast of the marks left in the clay by the foam tendrils and to provide a permanent record.

Circles of known diameter were arbitrarily drawn directly on the photocopied images. Care was taken to ensure that the circles fell completely within the field of the image. The diameter of the circle was chosen to provide approximately 35 counts or intersections with the pore boundaries. (Ref. 51, 52)

Intersections of the circle and each pore boundary were marked directly on the image. An intersection of the circle with a pore boundary was given a count of 1. When the circle coincided with a junction of three pores that intersection was given a count of 2. After all intersections were marked along the circumference of the circle a total count was made.

The average number of counts per circle was determined for each specimen. The average pore diameter, p_{avg}, was then calculated by

$$p_{avg} = \frac{\pi D / Mag}{\bar{N}} \qquad [28]$$

where $\bar{N}$ is the average number of counts, D is the diameter of the circle, and Mag is the magnification of the image used.

Procedure for measuring volume fraction

The volume fraction of each foam specimen was determined by the ratio of mass to bulk volume. Each specimen was weighed on an analytical balance to a resolution of 0.00001gm. The bulk volume was determined by measuring the volume of the test cell with water. The Plexiglas plate with a single 1/4" hole was screwed to the top of the chamber to provide a constant volume. Water from a graduated burette was used to fill the test cell volume. The test chamber was considered full when water reached the bottom of the filling hole and no air bubbles remained. The volume ratio of the foam was determined as the ratio of mass volume to bulk volume. The ratio, presented here as Equation [29], is given as

$$\%\ vol.\ fraction\ = \frac{mass}{Vol_{bulk}\rho_{Al_{6061}}} \qquad [29]$$

where $\rho_{Al_{6061}}$ is the density of 6061 aluminum, *mass* is the test cell volume measured, and Vol_{bulk} is the bulk volume in milliliters.

Estimated errors in measurement

Measurement errors that might be expected to occur in this experiment come from a variety of sources. The major sources of error include agreement of experimental values with thermal conductivity values for standard materials, reproducibility of results, contact resistance, penetration depth of the heat flux, and additional modes of heat transfer including convection and radiation.

Standard material testing

In order to determine the accuracy of the test fixture, a standard material was tested and the results compared to its reference thermal conductivity. Water was chosen as the reference material due to its well-measured thermal conductivity, availability, and as use as an baseline measurement against which the test specimens of foam+water could be compared.

Calibration with water as a test material

Water represented the lower thermal conductivity limit required for the test equipment for this experiment. Water at room temperature (25°C) has a thermal conductivity of 0.607 $^{W}/_{mK}$. (Ref. 49)

The results of tests on water yielded an averaged thermal conductivity of 0.597 at an initial temperature of 22°C. The standard error of the test results was 0.01200. This compares with an interpolated value for water at 22°C of 0.602 $^{W}/_{mK}$ calculated from values in the CRC Handbook of Chemistry and Physics (Ref. 49). The difference between the measured value and the interpolated value is 1%.

Effects of convection in measurements

The testing of water allowed the effects of convection to be studied. It was observed in the results of the tests that the orientation of the strip effected the variance in the data. It was determined that a horizontal orientation for the heater strip, ie. with the strip faces parallel to the floor, resulted in the most consistent results. Therefore all subsequent testing was done with the heater strips in the horizontal configuration.

Analysis of the data indicated that near the end of the test period the relationship between the measured resistance and the time function $f(\tau)$ ceased to be linear. It was determined that this was due to the onset of convection. This effect was not seen when the material being tested was a solid or solid/liquid system (foam+water). Water tests were run with an abbreviated test period of approximately 18 seconds compared to a standard test period of 25 seconds. The results of the abbreviated tests indicate that prior to the onset of convection the method is accurate and valid for the testing of fluids at this thermal conductivity range. Figure 20 shows a data set for water alone where the effect of convection on the results is apparent.

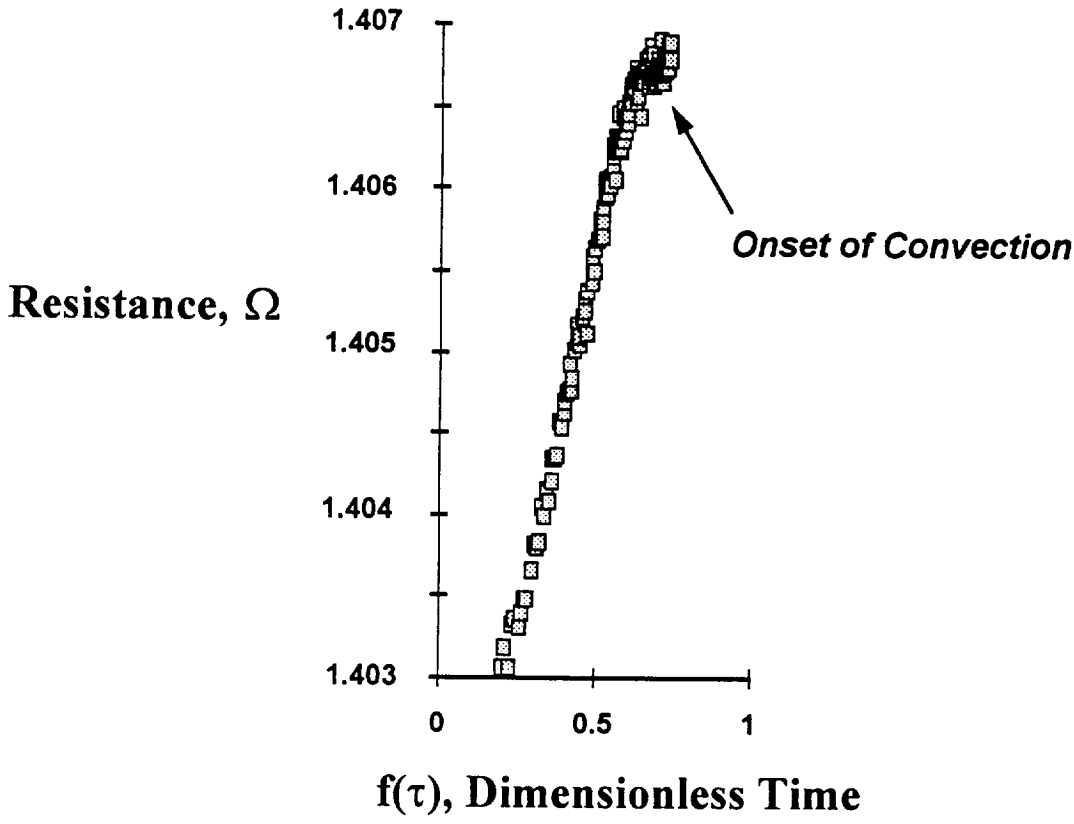

Figure 20. Data showing onset of convection in water-only sample

Error due to specimen thickness

Implicit in the Transient Hot Strip method is the assumption of infinite specimen thickness in the direction of the heat flux. This is a direct requirement of the one dimensional heat flow in the specimen. It has been shown in previous works by Gustafsson (Ref. 39) that the probe depth, Æ, can be defined as

$$\Delta = 1.42\sqrt{at} \qquad [30]$$

where a is the diffusivity and t is the measurement time.

Additionally, according to Log and Metallinou, (Ref. 53) in actual experiments the probe depth was determined to be approximately equal to the width of the heater strip, 2d. Therefore, the thickness of the specimens in this study must be at least 12mm since the heat flux flowed from the center of the specimens equally in the positive and negative z-directions. The dimensions of the specimens in the direction of heat flow (z-direction) averaged 18mm.

Error due to contact resistance

Contact resistance was minimized by using a wooden (non-conductive) wedge to firmly press the two specimen slabs against the heater strip. The error due to non-uniform contact resistance can be determined by comparing the variance in results from tests using the same experimental set-up (ie. repeated testing without re-installing the specimen in the test fixture) to results of independent replications (complete removal and installation for each test). The variance between repeated tests was 0.0110. This compares to a variance of 0.0197 for replicated tests on the same specimens. The error due to changes in contact resistance was assumed to be the difference between the replication and repeated test variances. The difference in the variances was 0.0087, which represents the error due to changes in the contact resistance. All test data reported were from replicated testing.

Error due to radiative heat transfer

The error due to neglecting heat flow due to radiation can be calculated by determining the ratio of radiative versus conductive heat flow. (Ref. 54) Using the general equations for radiative and conductive heat transfer yields the ratio

$$\frac{radiation}{conduction} = \frac{4\sigma\varepsilon T_{avg}^3 P}{\lambda_{eff}} \qquad [31]$$

where ε represents the emissivity, σ is the Stephan-Boltzmann constant, T is the test temperature in Kelvin, P is the average pore diameter, and λ_{eff} is the effective thermal conductivity. The emissivity for the system was on the order of 1.0 the temperature was 325K, the largest average pore size was 3.9 mm, and the effective thermal conductivity was 2.0 W/mK. The ratio of radiative to conductive transfer was calculated as

$$\frac{radiation}{conduction} \approx 0.4\% \qquad [32]$$

therefore the effect of radiation can be neglected without a significant sacrifice in accuracy.

Results

Using the experimental procedures outlined in the previous section, the effective thermal conductivity for the nine aluminum foam+water specimens, plus water alone, were measured. In addition to the effective thermal conductivity measurement, the average pore sizes and volume fractions of the same nine aluminum foam samples were measured. The average values for these measurements were used to generate predictions for each of the ten effective conductivity models presented earlier.

In this section the results are presented. This is followed by a Discussion section where these experimental results are reviewed, placed under statistical scrutiny, and then used to predict reductions in the time to freeze using an aluminum foam over water alone.

The nine specimens were nominally of three volume fractions of foam, 4, 6, and 8%, crossed with three pore sizes, 10, 20, and 40 pores per inch (2.5, 1.3, and 0.6 mm). Each specimen was therefore labeled in this report with its nominal volume fraction and pore size; for example, the 4%, 10 pore per inch specimen is labeled as specimen 410.

Results of effective thermal conductivity measurements

The measured effective thermal conductivity for the nine aluminum foam and water specimens are presented in Table 5. The calculated effective thermal conductivity and standard error are also listed.

Table 5. Effective thermal conductivity for the nine foam+water specimens

Specimen	Raw data										Average	Std. dev.
410	1.23	1.29	1.31	1.35	1.22	1.19	1.25	1.26	1.29	1.29	1.27	0.05
420	1.63	1.44	1.52	1.57	1.50	1.46	1.43	1.50	1.49	1.64	1.52	0.07
440	1.38	1.34	1.34	1.84	1.35	1.36	1.41	1.36	1.43	1.39	1.42	0.15
610	1.68	1.69	1.77	1.76	1.67	1.68	1.77	1.79	1.61	1.63	1.70	0.06
620	1.47	1.52	1.66	1.59	1.47	1.48	1.48	1.39	1.33	1.48	1.49	0.09
640	1.72	1.78	1.88	1.83	1.77	1.90	1.93	1.77	1.71	1.76	1.80	0.07
810	1.55	1.36	1.27	1.48	1.56	1.37	1.20	1.59	1.42	1.31	1.41	0.13
820	1.83	1.94	2.49	2.21	1.85	1.74	1.78	1.78	1.59	1.31	1.85	0.32
840	2.39	2.52	2.45	2.44	2.37	2.20	2.46	2.28	2.31	2.38	2.38	0.09
Water	0.673	0.570	0.598	0.605	0.508	0.558	0.491	0.565	0.549	0.553	0.596	0.05
	0.606	0.696	0.613	0.600	0.612	0.633	0.650	0.638	0.616			

Results of volume fraction measurement

The volume fraction of each of the nine aluminum foam specimens was measured and are presented in Table 6.

Table 6. Results of volume fraction testing

Nominal Pore Size	Nominal Volume Fraction: 4% Al Foam		Nominal Volume Fraction: 6% Al Foam		Nominal Volume Fraction: 8% Al Foam	
2.5mm	Volume Fraction:	3.7%	Volume Fraction:	6.1%	Volume Fraction:	7.7%
1.3mm	Volume Fraction:	5.2%	Volume Fraction:	5.6%	Volume Fraction:	7.8%
0.6 mm	Volume Fraction:	3.8%	Volume Fraction:	6.0%	Volume Fraction:	8.4%

Results of pore size measurement

The results of measuring the average pore size for the nine specimens using ASTM method E112-88 are presented in Table 7 below. In the table, the measured average pore size and standard error are given for each specimen.

Table 7. Results of Average Pore Size Measurement

Nominal Volume Fraction

Nominal Pore Size	4% Al Foam		6% Al Foam		8% Al Foam	
2.5mm	Avg. Pore Size (mm):	3.94	Avg. Pore Size (mm):	2.91	Avg. Pore Size (mm):	3.89
	Std. Error:	0.125	Std. Error:	0.079	Std. Error:	0.154
1.3mm	Avg. Pore Size (mm):	2.51	Avg. Pore Size (mm):	2.93	Avg. Pore Size (mm):	2.73
	Std. Error:	0.077	Std. Error:	0.106	Std. Error:	0.077
0.6 mm	Avg. Pore Size (mm):	2.08	Avg. Pore Size (mm):	2.15	Avg. Pore Size (mm):	2.06
	Std. Error:	0.000	Std. Error:	0.047	Std. Error:	0.046

In this section the results of testing for the average pore size, volume fraction of the aluminum foam, and the effective thermal conductivity of the foam+water specimens were reported. Using these results, predictions of the effective thermal conductivity were calculated using the theoretical models. The bounding models; the Arithmetic Mean, Harmonic Mean, and Maxwell's Upper and Lower Bounding models, and the Geometric Mean model used the experimentally determined volume fractions to predict the conductivity. The unit cell model by Dulnev used the results of the average pore size and the average tendril diameter of the aluminum foam in order to predict an effective thermal conductivity. The remaining four models by Hadley, Asaad, de Vries, and Zumbrennen, Viskanta, and Incropera used the volume fraction s and the measured effective thermal conductivities to fit the empirical coefficients. The correlation coefficients adjusted the predicted values to approximate the measured results.

In the next section the experimental results are analyzed to determine the relationships between the pore size and volume fraction to the effective thermal conductivity. The predictions calculated from the theoretical models will be compared to the experimental results.

Predictions based on theoretical models

The experimental results presented above were used to calculate predictions for the effective thermal conductivity from the models presented in the Background section. These were calculated based on the test results of the volume fraction and average pore size of the aluminum foam specimens, and the effective thermal conductivities measured from the foam+water specimens.

The experimentally determined volume fractions were used to develop each of the equations except for the model by Dulnev which used only the results of the pore size measurement.

The experimentally determined thermal conductivities were used to optimize the models by Asaad, Hadley, de Vries and Zumbrennen, Viskanta, and Incopera. The correlation factors in each of these models; c, for Asaad; α and f for Hadley; F for De Vries; and φ for Zumbrennen, Viskanta, and Incopera, respectively, were optimized in order to more closely align the model predictions with the actual measured conductivities.

Bounding equations

The effective thermal conductivities predicted by the four bounding equations are presented in Table 8. The volume fraction of the interlacing aluminum foam material measured previously was used to produce an effective conductivity. Graphically the bounding equations are shown in Figure 21.

Table 8. Effective thermal conductivities for four models

Exp'l Results			Theoretical Models			
Specimen ID	%Volume Fraction, Foam	Eff. Th. Conductivity	Arithmetric	Harmonic	Upper Maxwell	Lower Maxwell
410	3.7%	1.27	5.62	0.63	4.00	0.68
420	5.2%	1.52	7.67	0.64	5.41	0.71
440	3.8%	1.42	5.79	0.63	4.12	0.68
610	6.1%	1.70	8.92	0.65	6.27	0.73
620	5.6%	1.49	8.23	0.65	5.80	0.72
640	6.0%	1.80	8.85	0.65	6.23	0.73
810	7.7%	1.41	11.0	0.66	7.76	0.76
820	7.8%	1.85	11.2	0.66	7.89	0.76
840	8.4%	2.38	12.0	0.66	8.43	0.77
		SSE	496	9.87	202	8.46

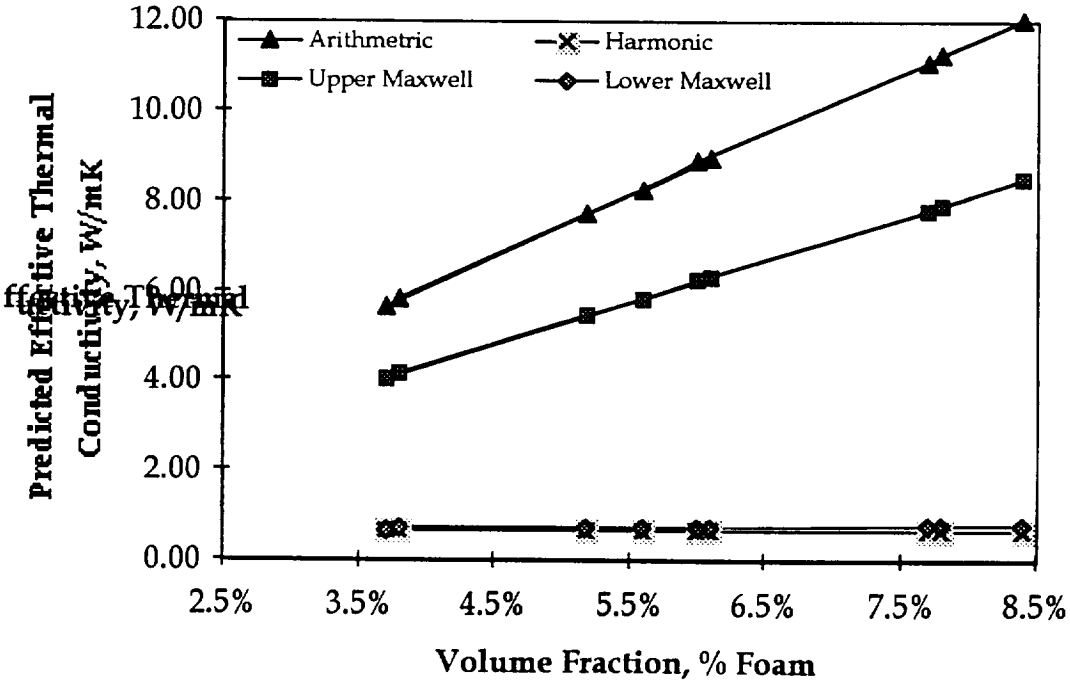

Figure 21. Predicted effective thermal conductivity using four different

Other models

Predictions for the effective thermal conductivity of the aluminum foam+water system were also generated by the remaining six models. The experimentally determined volume fractions were used with each model except the Dulnev model which used the average pore size. Additionally, the effective thermal conductivity measured experimentally was used to optimize the models by Asaad, Hadley, De Vries, and Zumbrennen, Viskanta, and Incopera. The thermal conductivities predicted by each of these six models are presented in Table 9. The empirical coefficients used for some models are also listed at the end of the table. A complete explanation of how these coefficients were determined in given in Appendix 2.

Table 9. Effective thermal conductivity predictions by six models

	Exp'l Results		Theoretical Models					
Specimen ID	%Volume Fraction, Foam	Eff. Th. Conductivity	Geometric	de Vries	Asaad	Dulnev	Zumbrennen, et al	Hadley
410	3.7%	1.27	0.74	1.13	1.32	1.24	1.47	1.16
420	5.2%	1.52	0.81	1.35	1.42	2.09	1.48	1.36
440	3.8%	1.42	0.75	1.15	1.33	3.29	1.47	1.18
610	6.1%	1.70	0.85	1.49	1.48	1.42	1.49	1.49
620	5.6%	1.49	0.82	1.41	1.45	1.69	1.49	1.42
640	6.0%	1.80	0.85	1.48	1.48	2.13	1.49	1.48
810	7.7%	1.41	0.92	1.73	1.60	0.78	1.50	1.69
820	7.8%	1.85	0.93	1.75	1.61	1.22	1.50	1.71
840	8.4%	2.38	0.96	1.84	1.65	1.85	1.50	1.78
		SSE	6.44	0.68	0.8	4.12	1.09	0.71

Coefficients

Asaad	c = 0.89
Hadley	α= 0.04 f= 0.082
De Vries	F= 0.100
Zumbrennen et al	ψ= 0 h(rad)= 0 φ= 0.63

These same data are presented in graphical form in Figure 22.

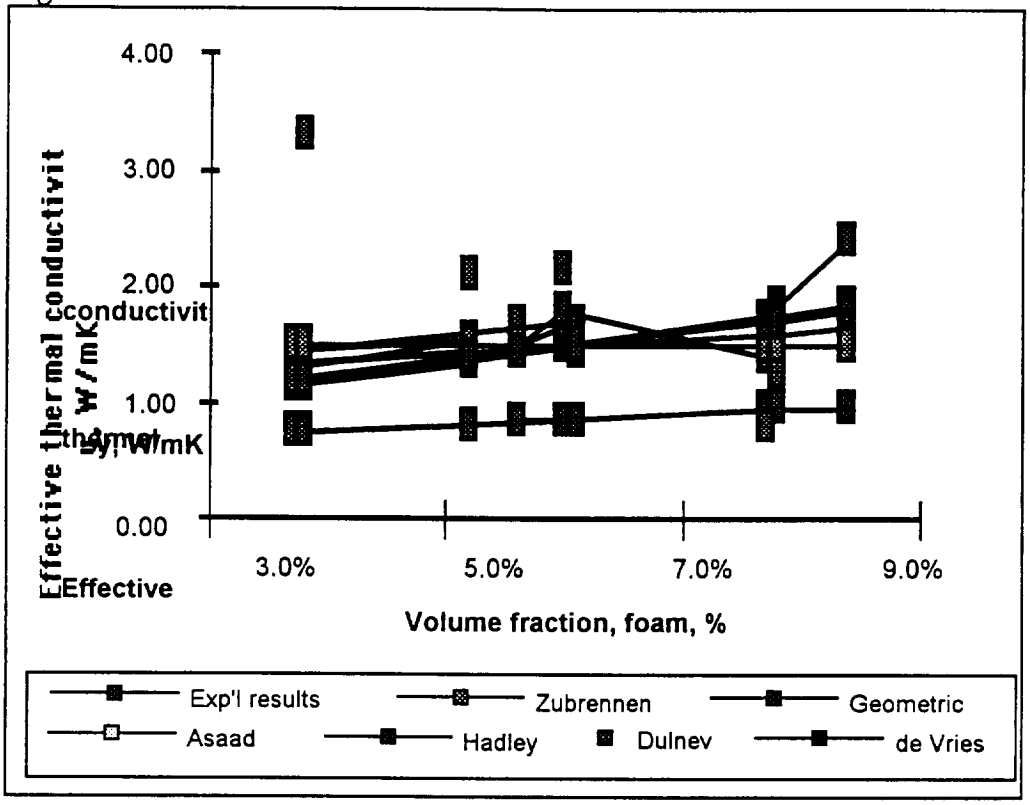

Figure 22. Predicted effective thermal conductivity values for six models

Discussion

In this section the experimental results were analyzed to determine the validity of the data. Analysis in the form of linear, higher order, and multiple variable regression analysis was performed on the data to determine the correlation of the volume fraction and pore size to the effective thermal conductivity. The regression analysis provided the statistical power to adequately compare the theoretical predictions to the experimental measurements.

Are the experimental results reasonable?

In order to begin a discussion of the relationships between the factors that have been tested, the data was first scrutinized for reasonable results.

The values calculated for the three factors were mean values of a given number of replications. These mean values should be reasonable compared to the expected values assumed at the start of the experiment. The mean values determined for the volume fraction, average pore size, and effective thermal conductivity also have a variance associated with the value reported. The variation or spread around the mean value is an indication of whether the mean values are significantly different from the others so that distinctions between samples can be made.

Volume fraction

Measurements of the percent volume fraction of foam relied ultimately on the differences in masses of the individual specimens. To determine the volume fraction of each piece of aluminum foam, the mass of the specimen was multiplied by a constant value proportional to the volume of test fixture and the density of the parent (6061 AL) material.

The use of mass to determine volume fraction relied on the assumption that the overall volume (foam + pore volume) that the foam encompasses was equal in each case. Additionally, it was assumed the foam was generally isotropic and homogeneous. These conditions were

Average pore size

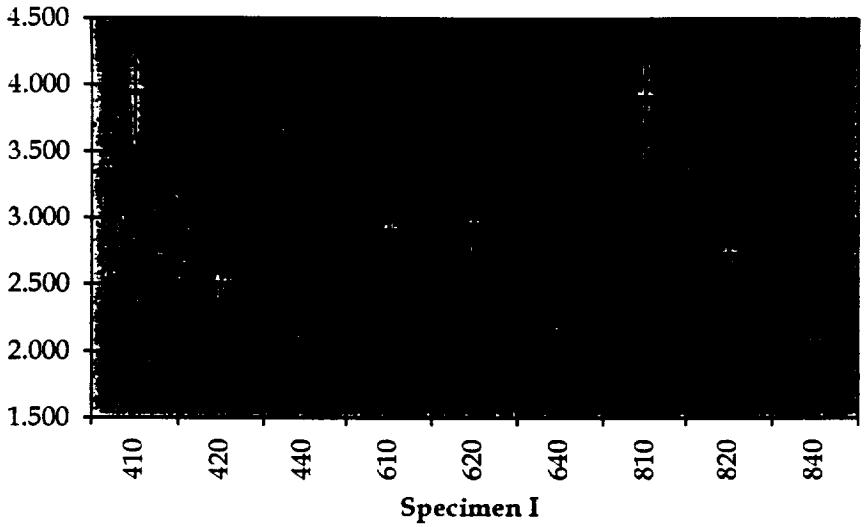

Figure 23. Average pore size measurement

Thermal conductivity

Reasonable?

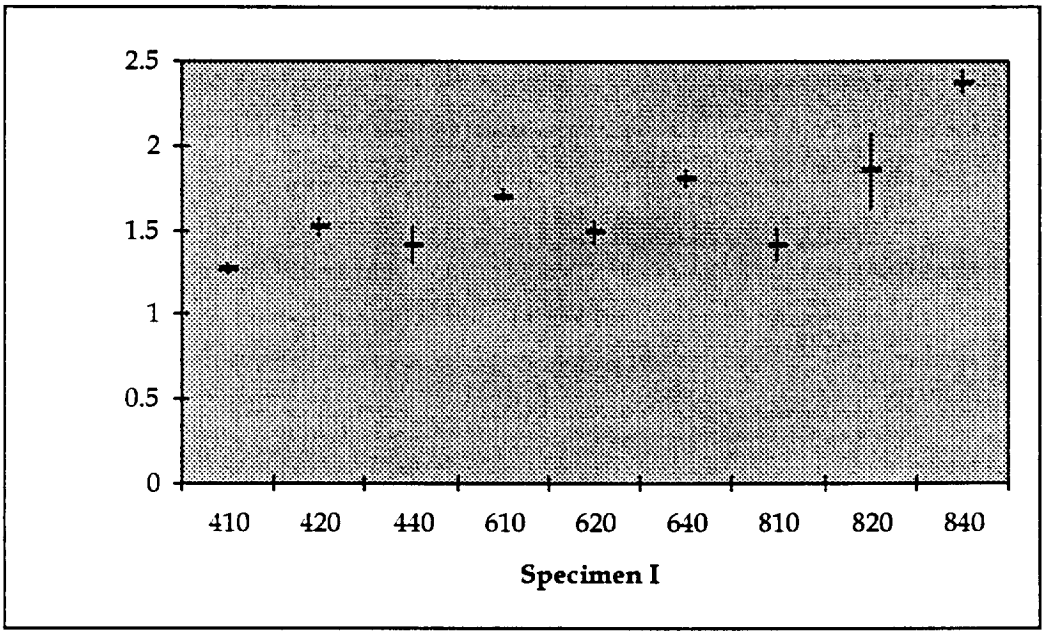

Figure 24. Experimental results of thermal conductivity with error bars

Correlating experimental results

To determine whether a correlation existed between the effective thermal conductivity and the volume fraction or average pore size the following steps were taken:

- Produced graphs of effective conductivity versus volume fraction and effective conductivity versus pore size.
- Observed general relationships.
- Determined independent linear relationships.
- Performed tests for a linear correlation.
- Performed tests for higher order terms.
- Determined confidence intervals.

A multiple regression analysis was performed to determine the interaction between the volume fraction and the pore size on the effective conductivity.

Effect of volume fraction on the effective thermal conductivity

The relationship between the volume fraction and the effective thermal conductivity was graphed in Figure 25. As expected, increases in the volume fraction of the aluminum foam resulted in increases in the thermal conductivity of the system. This trend can be seen clearly in the Figure below.

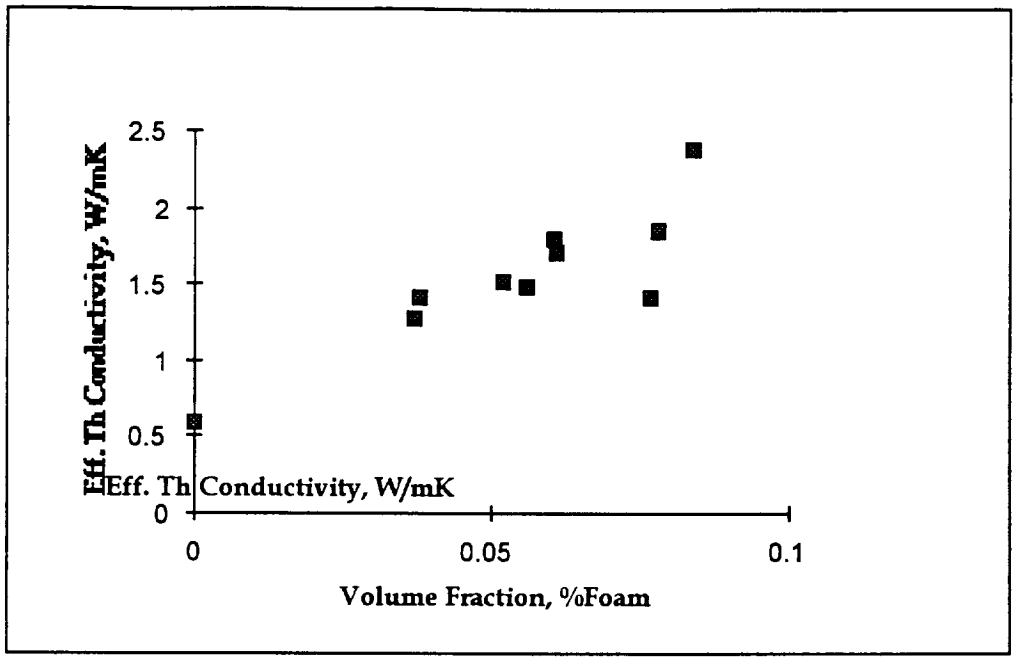

Figure 25. Experimental results of thermal conductivity measurement as a function of volume fraction

A linear relationship between the volume fraction and conductivity was assumed and a single factor regression analysis was performed. The straight line equation of conductivity as a function of volume fraction is presented here as Equation [34]

$$\text{Th Conductivity} = 15.255(\text{vol frac}) + 0.66309 \qquad [34]$$

A test for the utility of the regression equation was performed on the slope. A 95% confidence interval test resulted in a value of 30.51. This result compared to a rejection value of 2.00 for the slope indicated that it was statistically relevant that the effective thermal conductivity increased with increasing volume fraction. The data with the regression line overlaid is shown in Figure 26.

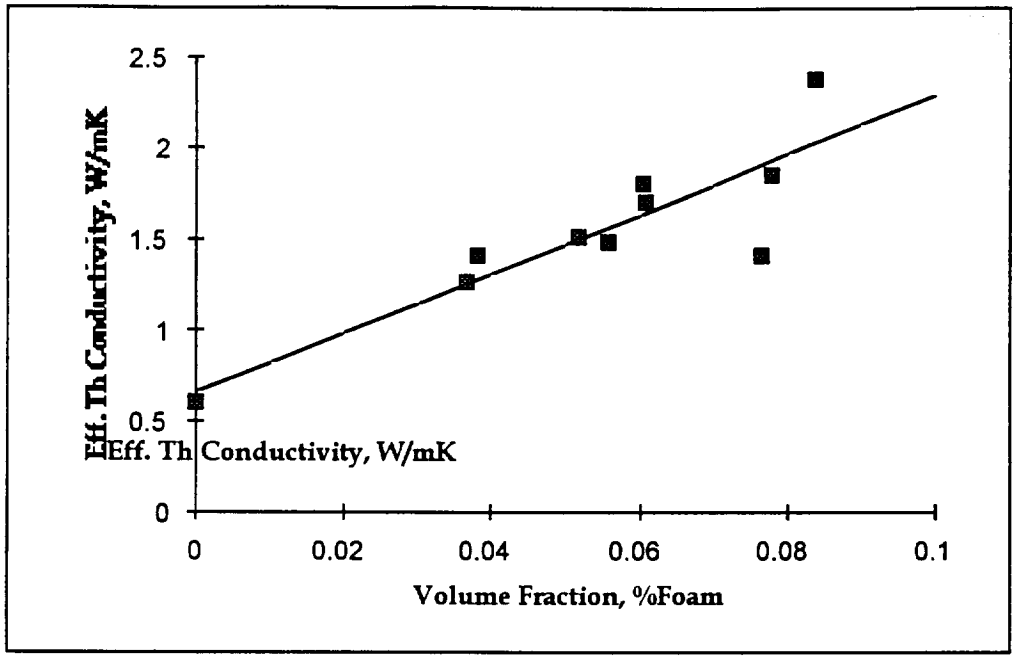

Figure 26. Effective thermal conductivity as a function of volume fraction

The r^2 coefficient of determination for the conductivity to volume fraction data was determined to be 0.77. Hence, 77% of the variation in the effective thermal conductivity measured can be attributed to changes in the volume fraction. (Ref. 55)

Second order regression

A second order regression of the independent variable, volume fraction, was performed on the data to determine the effects of higher order terms. The second order regression equation, presented here as Equation [35], for the volume fraction was determined to be

$$Th\ Cond. = -28.476(vol.\ frac)^2 + 18.731(vol.\ frac) + 0.6282 \quad [35]$$

Student's t-test was used to determine whether the higher order term was statistically beneficial in predicting the effective thermal conductivity. The null hypothesis for the test was

$$H_o: \ 2nd\ Order\ Coefficient = 0$$

$$H_a: \ 2nd\ Order\ Coefficient \neq 0$$

$$test\ statistic \quad t = \frac{2nd\ OC}{s_{2nd\ OC}} = \frac{2nd\ OC}{s/\sqrt{SS_{xx}}}$$

$$t = 0.243$$

$$rejection\ region: \ |t| > t_{crit} = 2.365 \qquad [36]$$

The calculated t-value of 0.243 determined from Equation [36] was less than the critical value of 2.365, therefore the test was not able to reject the hypothesis. This indicates that the addition of higher order terms does not provide a better estimate of the correlation of volume fraction and effective conductivity.

Prediction interval for the effective thermal conductivity

The 95% prediction interval was determined for the volume fraction of foam as a predictor of the effective thermal conductivity. The upper and lower boundaries of this interval are shown in Figure 27. The symbols in the chart represent the measured thermal conductivities of this study, the solid line the best-fit linear equation, and the dashed lines the high and low (95%) prediction interval boundaries.

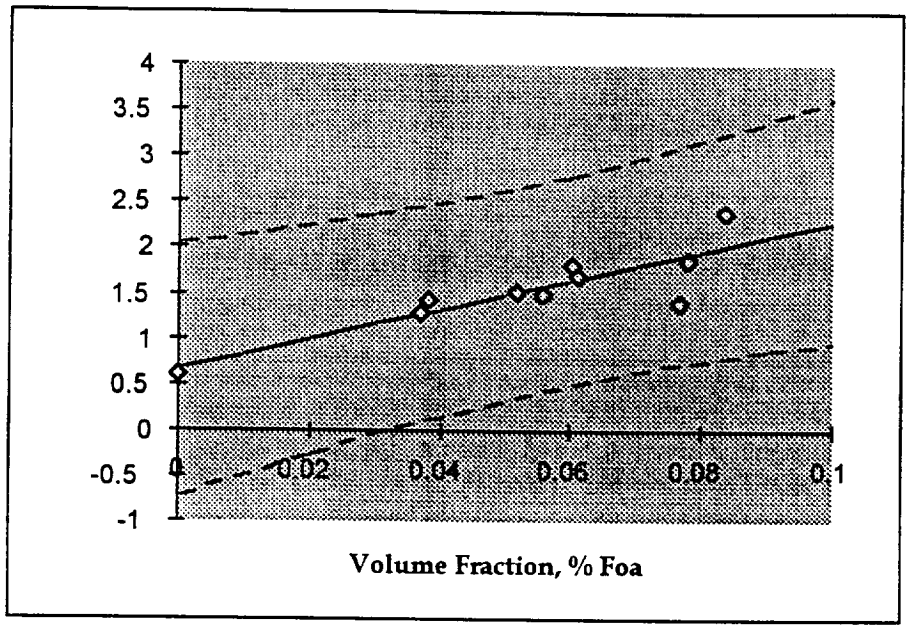

Figure 27. Effective thermal conductivity results with 95% confidence intervals added

The prediction interval maps the range of values within which an unknown sample's effective thermal conductivity would lie with a confidence value of 95%.

The prediction interval is quite large, ±0.843 W/mK at 5% volume fraction. This is probably due to the small size of the sample study. Larger samplings would decrease the width of the prediction interval. (Ref. 55)

The volume fraction was determined to have a strong linear correlation to the effective thermal conductivity. This agrees with the results predicted by the theoretical models in the earlier section. However, the r^2 correlation is not strong enough to draw the conclusion that volume fraction alone is significant enough to predict the effective thermal conductivity. The effect of pore size may also influence the effective conductivity. In the following sections the significance of this parameter is examined.

Effect of pore size on the effective thermal conductivity

The relationship between the average pore size and the effective thermal conductivity was determined in the same fashion as the volume fraction was in the previous section. The graph of the effective conductivity as a function of the average pore size is presented here as Figure 28.

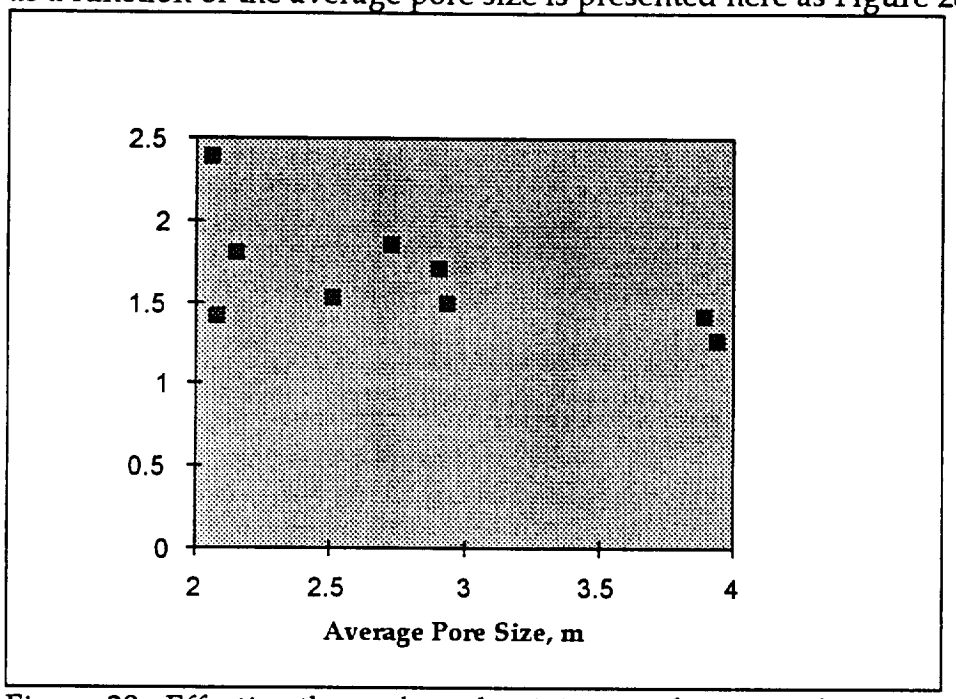

Figure 28. Effective thermal conductivity as a function of average pore size

A linear relationship was assumed between the thermal conductivity and the pore size. A linear regression analysis was performed which yielded the following straight line equation:

$$Th\ Conductivity = -0.2825(pore\ size) + 2.440 \qquad [37]$$

The slope of -0.2825 represents the trend of decreasing effective thermal conductivity with increasing pore size.

The r^2 coefficient of determination for this model was determined to be 36.4%. This is a low measure of correlation between the effect of increasing pore size and decreasing thermal conductivity.

A test of the utility of the straight line equation was performed. The null hypothesis was that the slope = 0; that the pore size had no linear effect on the effective thermal conductivity.

$$H_o: \ slope = 0$$

$$H_a: \ slope \neq 0$$

$$test\ statistic \quad t = \frac{slope}{s_{slope}} = \frac{slope}{s/\sqrt{SS_{xx}}}$$

$$t = -1.247$$

$$rejection\ region: \ |t| > t_{crit} = 2.365$$

The value of the 95% confidence t-statistic was determined to be t = -1.247. Compared to the critical t-value of t_{crit} = 2.365, the absolute value of the t-statistic was not greater and the null hypothesis failed to be rejected. Therefore the data was not able to substantiate the hypothesis that changes in the pore size correlated to changes in the effective thermal conductivity.

Failure to reject the null hypothesis can be attributed to three possible reasons; effects due to the volume fraction or interaction between the pore size and volume fraction, insufficient sampling size in the study, or no actual correlation of the conductivity with respect to the pore size.

The regression analysis performed above was for the independent relationship between the pore size and the effective conductivity. It has already been shown that changes in the volume fraction have a strong relationship to changes in the effective thermal conductivity. Interaction, or secondary, effects between the volume fraction and pore size may have contributed to the failure to show an independent correlation. A multiple variable regression analysis including both volume fraction and pore size

would allow these effects to be determined. Multiple variable regression will be discussed in the next section.

The number of observations in this experiment is nine. Small sampling sets such as with this experiment, decrease the magnitude of the t-statistic. Larger sample sizes provide a more accurate t-statistic. Given resources to include a larger number of observations a comprehensive study may indicate that pore size is significant to the effective conductivity.

No correlation between pore size and effective thermal conductivity may exist. In a strict one-dimensional heat flow model only the tendrils oriented in the direction of the heat flow would transport heat via axial conduction. All the other tendrils would participate in serial heat conduction in-line with the fluid. In areas much larger than the average pore size, the total cross-sectional area for parallel conduction either through the tendrils or through the fluid is constant with respect to pore size, assuming constant volume fraction. Likewise for serial conduction, the cross-sectional area available remains constant with changing pore size. Assuming first, strict, one-dimensional heat flow through the system, and second, the contributions of each heat pathway are additive, then there would be no change in the heat conduction with changes in pore size. Therefore, the result of no significance of conductivity to pore size changes in these experiments would agree with theoretical expectations.

Because of the strong correlation between the volume fraction and effective thermal conductivity the influence of pore size alone is not significant. Of course, this may not entirely discount any effect due to pore size. The next step to developing relationships between the variables and the

conductivity is by analyzing the two variable system in a multiple re analysis.

Multiple regression analysis

It must be considered that the unrejected test statistic for the was for the independent correlation of the pore size to the effective therma conductivity. It was shown previously that the volume fraction does h linear correlation to the effective conductivity. The effect of the v fraction and of possible interaction between the volume fraction and p size may influence the effect of pore size on the effective thermal conductivity.

A multiple variable regression analysis was performed using a complete second order equation to determine the main and secondary eff of volume and pore size on the effective conductivity. The form of th equation was

$$Th\ Cond. = \beta_0 + \beta_1 (vol.\ frac) + \beta_4 (pore) + \beta_2 (vol.\ frac)^2 + \beta_3 (pore)^2 + \beta_5 (pore)(vol.frac)$$

Tests of confidence in the β coefficients led to the removal of some of the terms. The final regression equation for volume fraction and pore presented here as Equation [38]

$$Th\ Cond. = \beta_0 + \beta_1 (vol.frac) + \beta_2 (pore)(vol.frac) \qquad [38]$$

where the β coefficients were determined to be

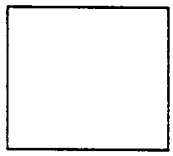

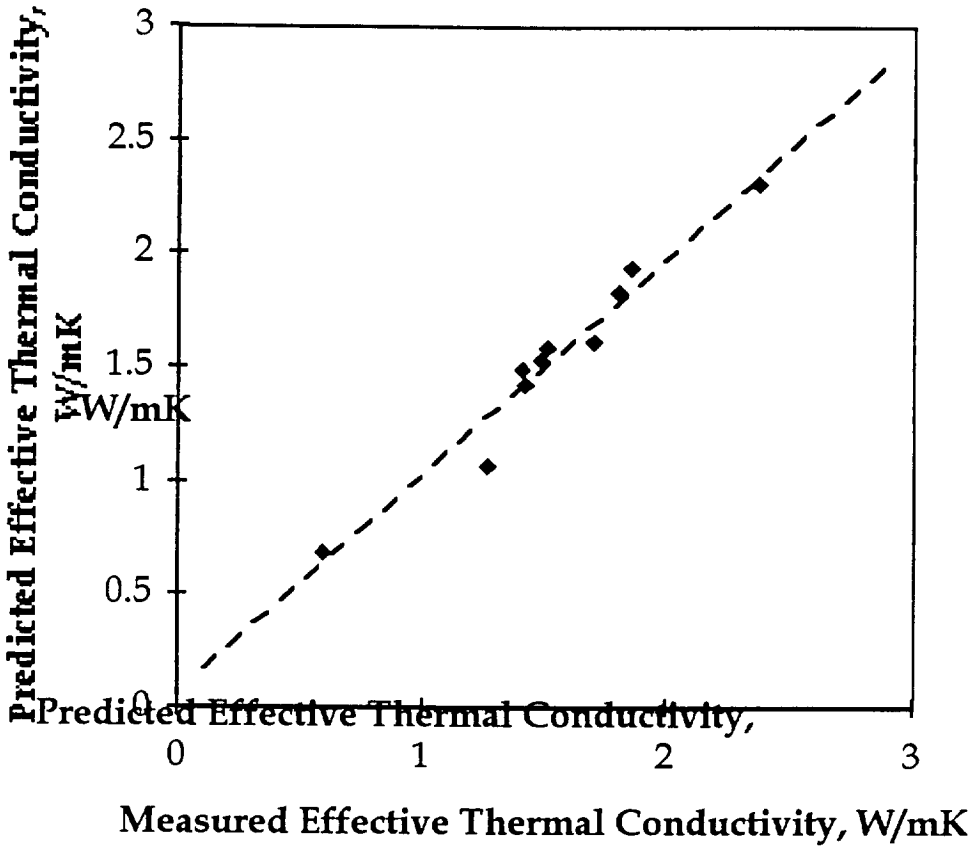

Figure 29. Predicted thermal conductivity versus experimental results

From the coefficient terms of the equation it is observed that the volume fraction and the interaction term between the volume fraction and the average pore size were the only significant terms in the correlation to the effective thermal conductivity. The average pore size was not a significant term and was removed to simplify the equation. A comparison of the predicted thermal conductivity using this regression model versus the measured thermal conductivity is shown graphically in Figure 29.

The r^2 coefficient of determination for this regression model was determined to be 0.96, or 96%. The r^2 values for correlating thermal

conductivity to volume fraction or pore size separately were 76% and 36%, respectively. Compared to the r^2 for volume fraction alone, we observe that using the additional information provided by the pore size, the predicted effective thermal conductivity can be substantially improved.

The multiple regression equation suggests that volume fraction is the primary parameter in determining the effective thermal conductivity. However, this relationship is not necessarily linear. The interaction term of the volume fraction and pore size modulates this effect which may suggest that conductivity is not a linear function of volume fraction but possibly logarithmic or some other function. It may also suggest that structure may be weakly influential, or that another, unspecified parameter may be influencing the results.

Theoretical models

The experimental results can now be compared against the models presented in the previous sections. Table 10 shows the experimental values of the volume fraction and effective thermal conductivity tabulated against the predicted values of each of the models. The sum of the squares of the error, SSE, for each model is included.

The range of predictions for the effective thermal conductivity was from a low of 0.63 to a maximum of 11.98 W/mK. The majority of the models predicted conductivity values in the range of 1.0-2.0 W/mK. The Sums of the Squares for Error, or SSE's, ranged from less than one to almost 500. An SSE value of zero signifies perfect correlation.

Table 10. Experimental effective thermal conductivity results and theoretical predictions based on the volume fraction measurements

Exp'l Results		Theoretical Models									
%Volume Fraction, Foam	Eff. Th. Conductivity	Arithmetric	Harmonic	Upper Maxwell	Lower Maxwell	Geometric	de Vries	Asaad	Dulnev	Zumbrennen	Hadley
3.7%	1.27	5.62	0.63	4.00	0.68	0.74	1.13	1.32	1.24	1.47	1.16
5.2%	1.52	7.67	0.64	5.41	0.71	0.81	1.35	1.42	2.09	1.48	1.36
3.8%	1.42	5.79	0.63	4.12	0.68	0.75	1.15	1.33	3.29	1.47	1.18
6.1%	1.70	8.92	0.65	6.27	0.73	0.85	1.49	1.48	1.42	1.49	1.49
5.6%	1.49	8.23	0.65	5.80	0.72	0.82	1.41	1.45	1.69	1.49	1.42
6.0%	1.80	8.85	0.65	6.23	0.73	0.85	1.48	1.48	2.13	1.49	1.48
7.7%	1.41	11.04	0.66	7.76	0.76	0.92	1.73	1.60	0.78	1.50	1.69
7.8%	1.85	11.22	0.66	7.89	0.76	0.93	1.75	1.61	1.22	1.50	1.71
8.4%	2.38	11.98	0.66	8.43	0.77	0.96	1.84	1.65	1.85	1.50	1.78
	SSE	496	9.870	202	8.456	6.435	0.683	0.798	5.117	1.085	0.709

Bounding equations

The experimental results for the effective thermal conductivity and the four bounding equations are graphed in Figure 30. As expected, plotting the experimental results and the bounding equations show that the experimental

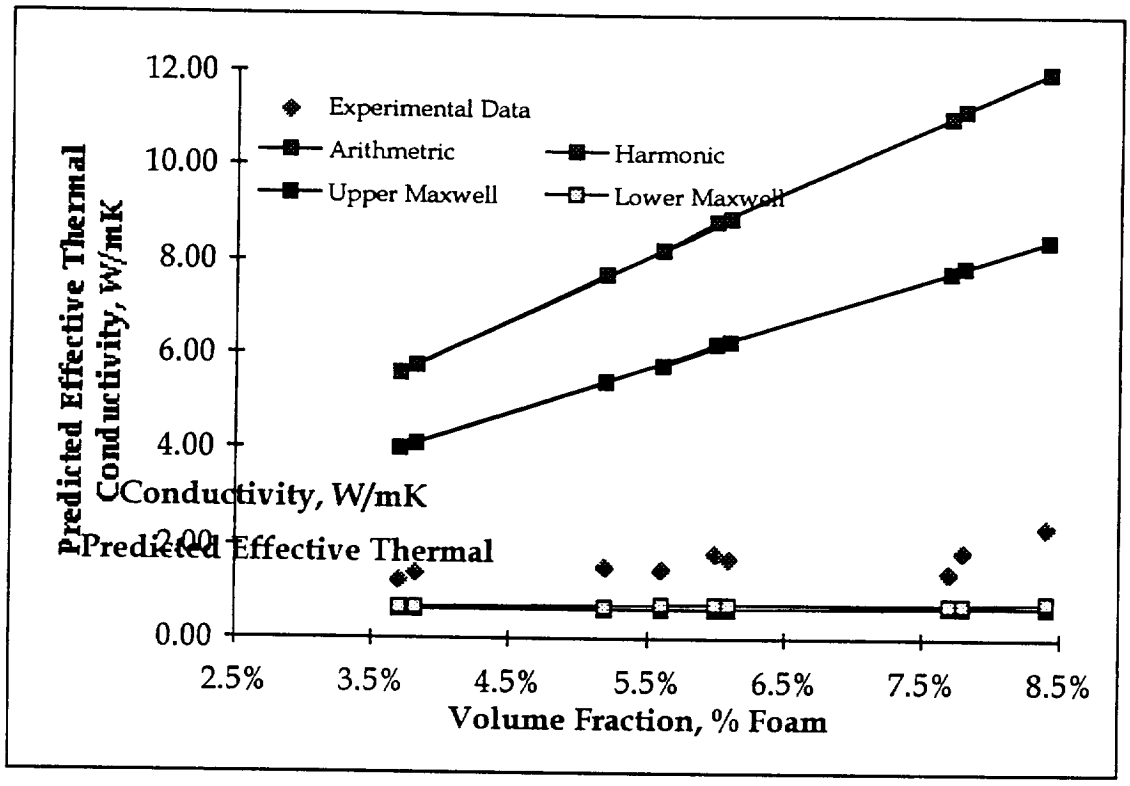

Figure 30. Experimental results plotted with bounding models

values lie within the limits of both the Arithmetic/Harmonic Mean models as well as the more stringent Upper and Lower Maxwell's bounding equations.

Comparison of theoretical predictions to experimental results

To compare the predictions to the experimental data a 95% confidence interval was used. The confidence interval defines a range of effective conductivities that lie within a 95% confidence interval for the true mean value. The confidence interval for the mean defines a more narrow range than the prediction interval presented earlier. (Ref. 55) Figure 31 presents the 95% confidence interval for the experimental data. The confidence interval can be seen to widen at either end of the range of conductivities

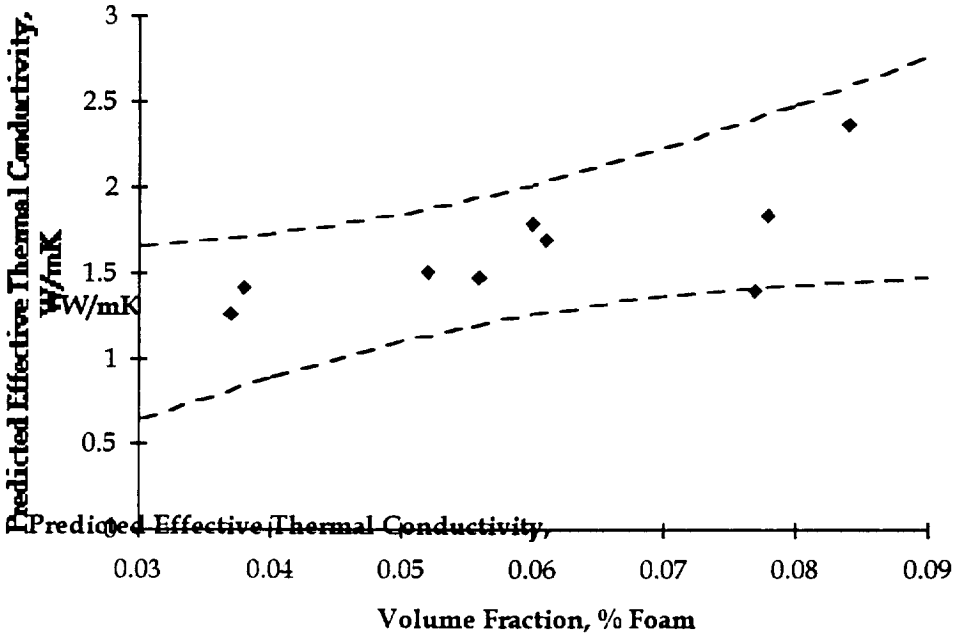

Figure 31. Experimental results versus volume fraction with confidence intervals

tested. This is due to the increasing distance from the average value of volume fractions tested.

The predictions generated by the models were compared against the experimental data and confidence intervals in order to determine the utility of the models. The comparison consisted of two steps, first, if a model prediction fell outside the confidence limits of the experimental data the model was judged to be not acceptable. Second, models whose predictions fell within the confidence limits were further tested to determine the statistical relevance of their slopes. A comparison of the slope of the regression line for the model was compared to the 95% confidence interval for the slope for the experimental values. Slopes that fell outside the confidence range were judged to be not acceptable models.

Models judged unacceptable because their predictions of the effective thermal conductivity fell outside of the 95% confidence limits were the Arithmetic, Harmonic, and Geometric Mean Models and the Upper and Lower Maxwell Equations. The Arithmetic Mean and the Upper Maxwell Equation fell above the upper limit while the other models had predictions that were below the lower limit. Figures 32 and 33 illustrate the positions of these models in relation to the confidence interval.

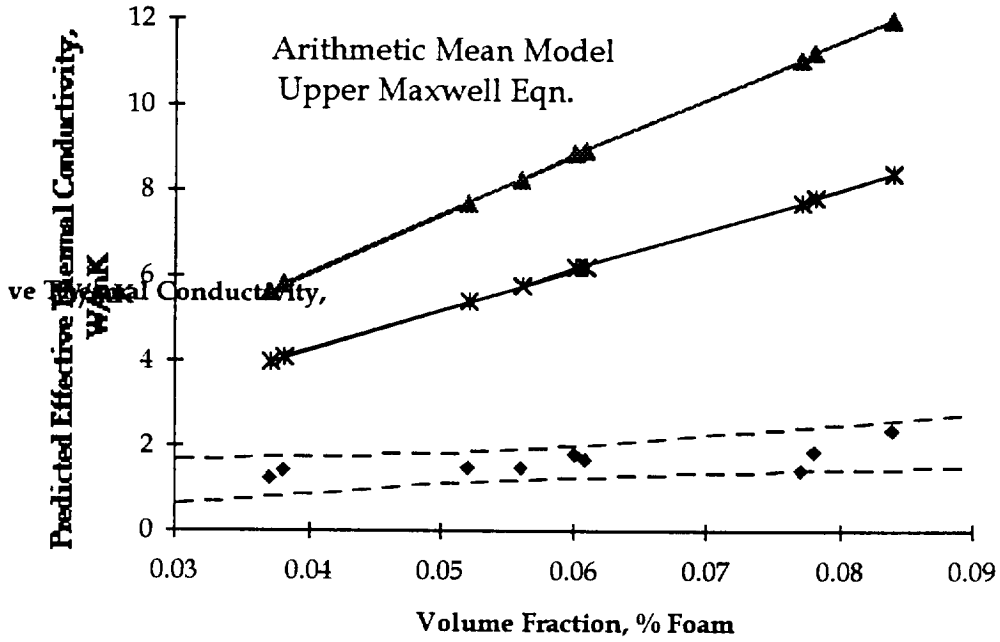

Figure 32. Predicted effective thermal conductivity of four models

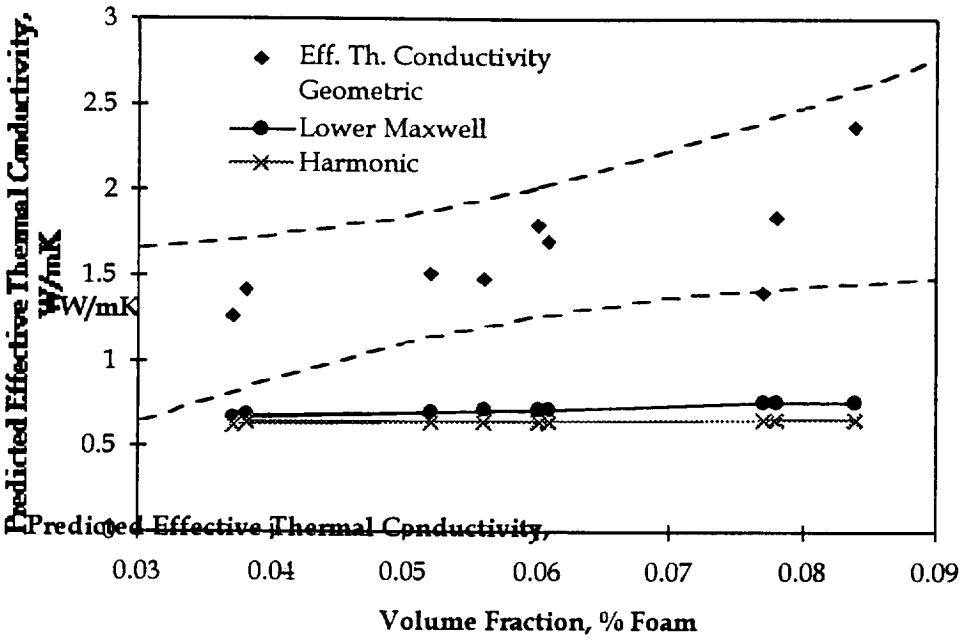

Figure 33. Predicted effective thermal conductivity of four models

Dulnev Unit Cell Model

The Unit Cell model by Dulnev presented an atypical result. From the graph of Dulnev's predictions in Figure 34, the predicted effective thermal conductivity predicted by the Dulnev model strongly relates increases in volume fraction of the aluminum foam to decreases in the effective conductivity. This inference to the relationship between volume fraction and conductivity is related to the use of the average pore size in determining the predicted values. As was demonstrated previously, pore size was mildly inversely proportional to the conductivity. Dulnev's predictions mirror these results.

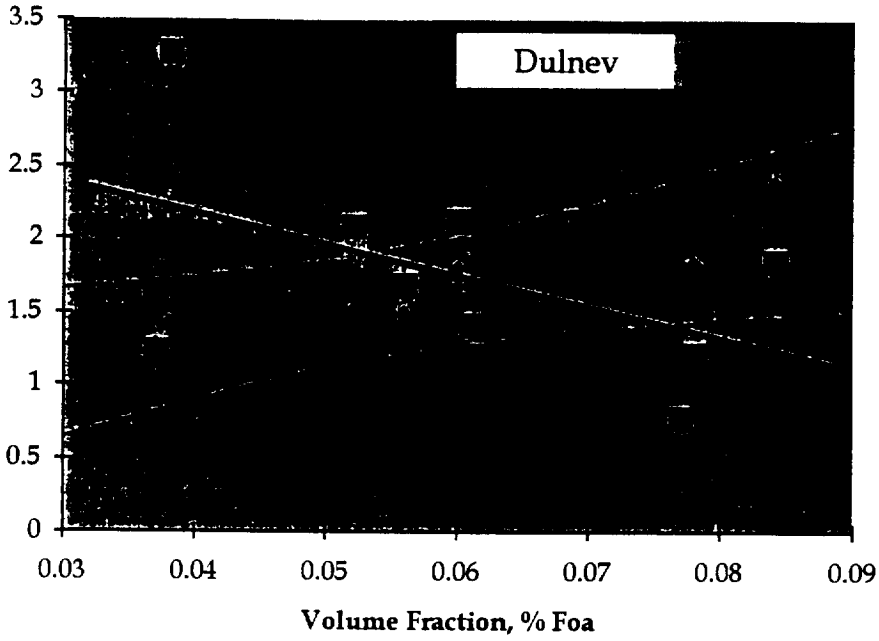

Figure 34. Dulnev predictions versus volume fraction compared to experimental results

The assumption made earlier in developing the Dulnev predictions was that the average pore size was equal in length to the body diagonal of the Dulnev cubic system. Tortuosity within the true foam cell, or the amount of deviation in the actual cell from the simplified model is probably high.

If the assumption between measured pore size and the characteristic unit cell is relaxed the unit cell length, L, can be determined empirically from the data. Graphing the sum of the squares for error as a function of unit cell length resulted in the plot shown in Figure 35.

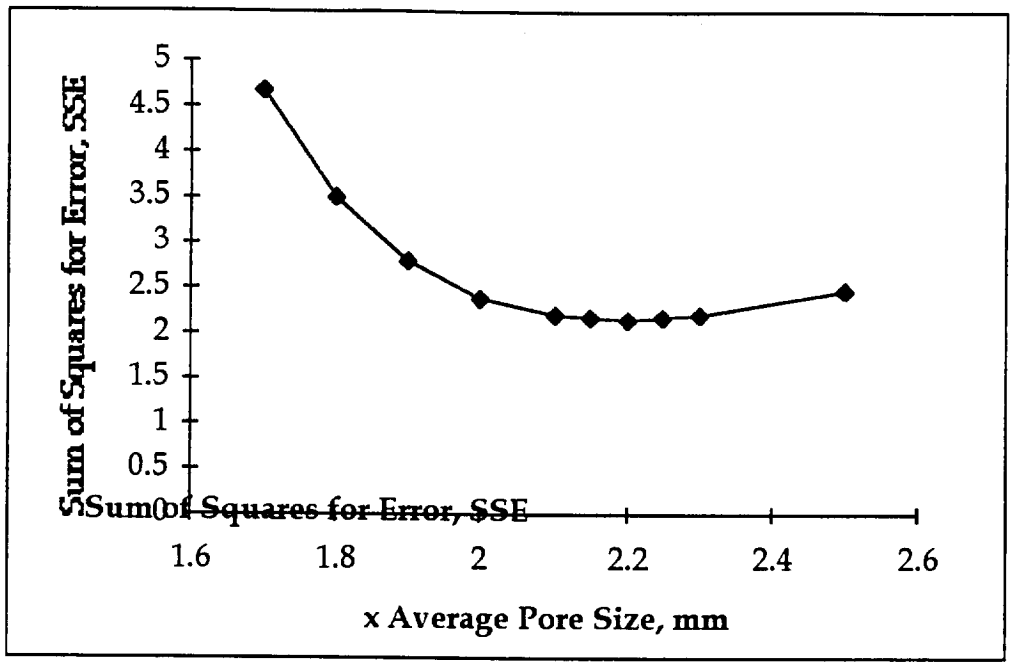

Figure 35. Sum of squares for error versus average pore size for Dulnev model

From the plot in Figure 35 the optimum value of the length of the characteristic unit cell was determined to be 2.20 x Pore Size. This optimum value suggests the tendrils of aluminum foam are less conductive than the parent material of which they are made.

Plotting the predictions of this optimized length value, which is presented as Figure 36, still resulted in an inversely proportional relationship between the volume fraction and the effective conductivity. Since the slope of this optimized line was still outside the 95% confidence interval for the experimental data the Unit Cell Model by Dulnev was deemed not acceptable.

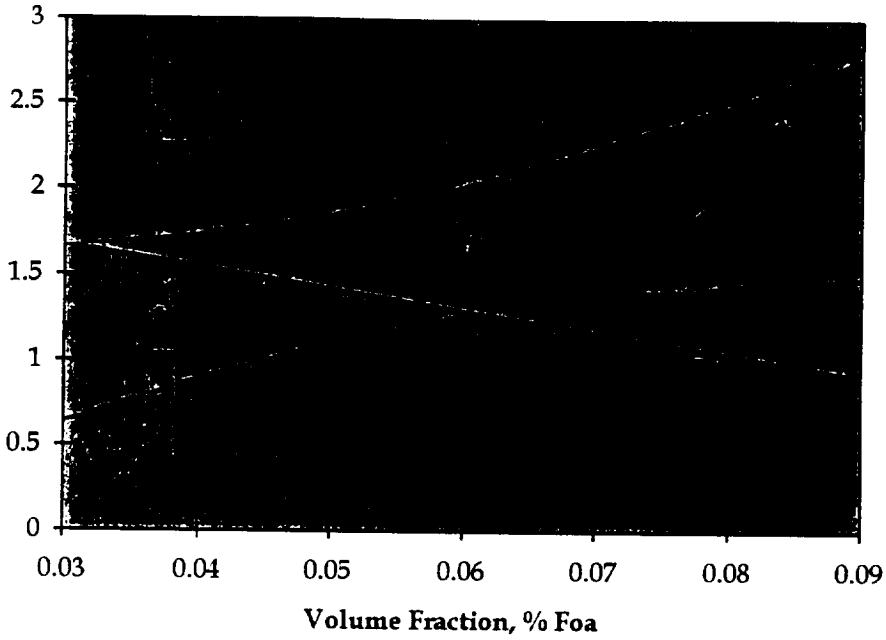

Figure 36. Predictions of effective thermal conductivity by Dulnev compared to experimental results

Determination of slope

The remaining four models; Asaad, Hadley, de Vries, and Zumbrennen, Viskanta, and Incropera each predicted conductivity values that were within the 95% confidence interval. Each of these models were then tested for the utility of their slope value. The equation of the line for each of the four model predictions were determined to be:

Asaad	$7.0701x + 1.0544$
Hadley	$13.131x + 0.6815$
de Vries	$15.124x + 0.5678$
Zumbrennen, Viskanta, and Incropera	$0.6673x + 1.4479$

In a previous section, the 95% confidence interval for the slope of the experimental data was found to range from 2.00 to 30.51. The graph in Figure 37 shows the agreement of the slopes of the models to this confidence

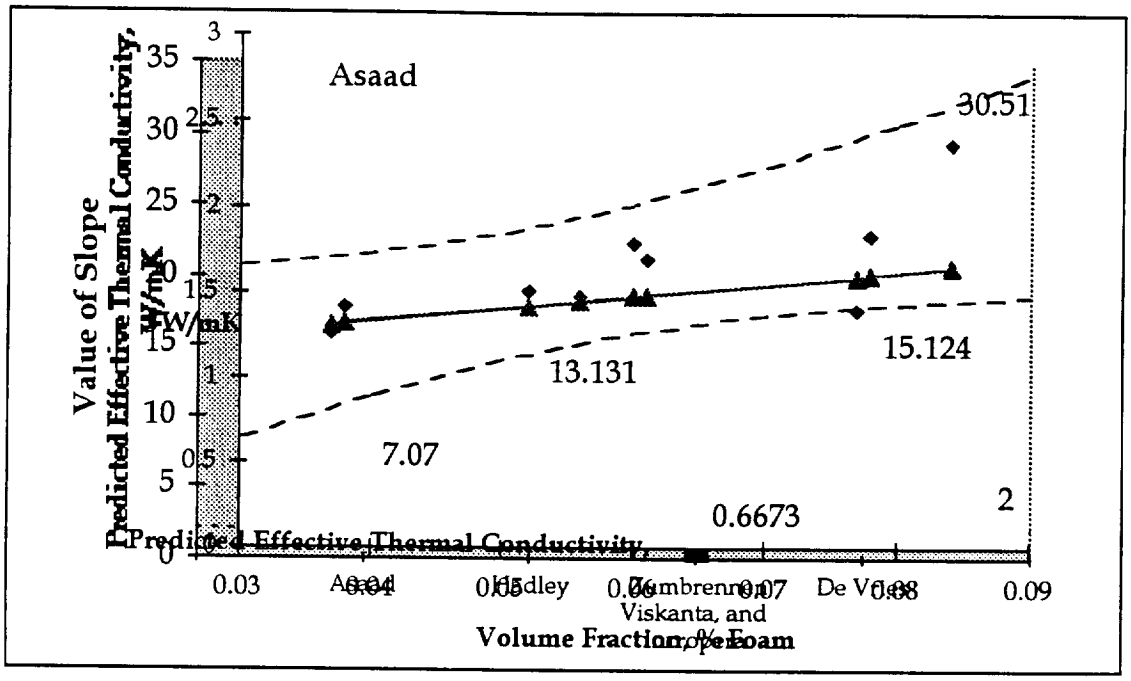

Figure 37. Slope values for four models compared to experimental confidence interval results

Figure 38. Asaad model predictions compared to experimental results

interval. The models of Asaad, Hadley, and de Vries each fall within the range of the slope interval. The slope of Zumbrennen, Viskanta, and Incropera lies outside the interval with a slope of 0.6673 compared to the minimum interval value of 2.00.

The three models; Asaad, Hadley, and de Vries were determined to satisfy the conditions of acceptance. Each model predicted values for the effective thermal conductivity within the 95% confidence interval and possessed values for their slopes that were within the limits of confidence of the slope for the experimental data. The graphs of Asaad, Hadley, and de Vries are presented in Figures 38, 39, and 40 respectively.

If we accept that the experimental data to be an accurate measurement of the effective thermal conductivity of aluminum foam and water systems

and that the Asaad, Hadley, and De Vries models can predict values for the effective thermal conductivity that lie within a specified confidence interval about these experimental data then we can use any of these models plus the multiple regression equation of the data to predict the effective conductivity for a given foam volume fraction and pore size. Following these predictions, the time to freeze, or regenerate, a system of foam + water can be estimated from the equations presented in an earlier section.

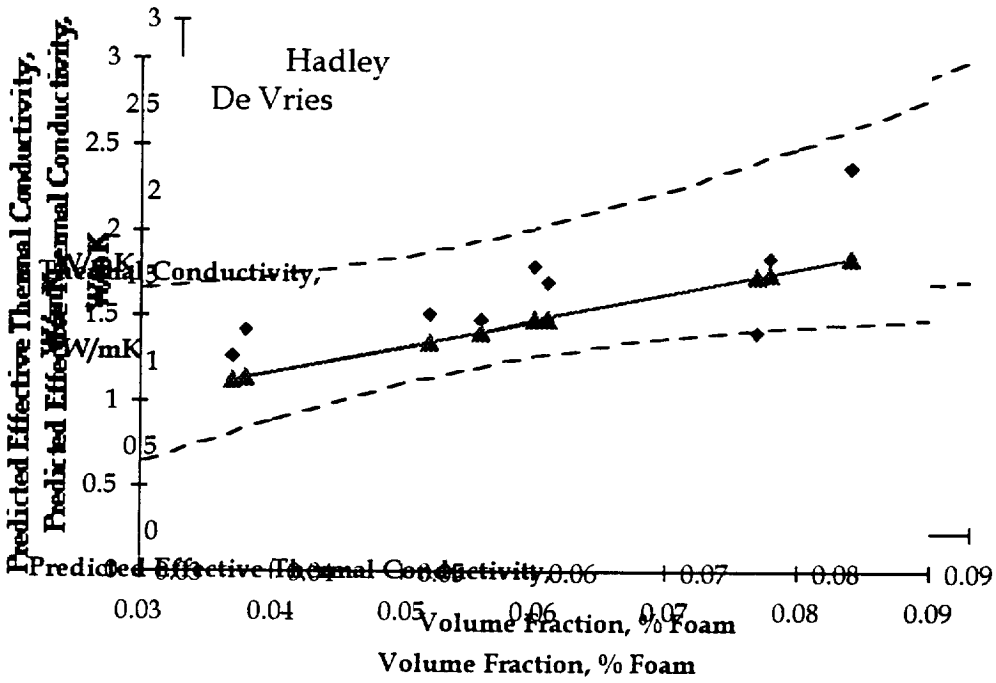

Figure 39. Hadley model predictions compared to experimental results

Figure 40. De Vries model predictions compared to experimental results

Using the models of Asaad, Hadley, and De Vries, the estimated effective thermal conductivity can be found for a set of foam+water systems. The predicted values are presented in Table 11. The foam parameters of volume fraction and pore size were arbitrarily selected but represent the range of conditions that may be possible using this particular foam product.

Table 11. Predicted foam+water effective thermal conductivities based on four equations

Pore size (mm)	Volume Fraction Solid %	Asaad (W/mK)	Hadley (W/mK)	De Vries (W/mK)	Experimental Regression (W/mK)	Average (W/mK)
2	4	1.41	1.07	1.23	1.47	1.295
4	4	1.41	1.07	1.23	1.28	1.198
2	6	1.55	1.32	1.55	1.86	1.571
4	6	1.55	1.32	1.55	1.28	1.426
2	8	1.71	1.57	1.89	2.26	1.827
4	8	1.71	1.57	1.89	1.48	1.663

Table 12. Predicted effective thermal conductivities from several models

Volume Fraction Solid, %	Asaad (W/mK)		Hadley (W/mK)		De Vries (W/mK)	
	Water	Ice	Water	Ice	Water	Ice
4	1.41	4.18	1.07	3.57	1.23	3.47
6	1.55	4.49	1.32	4.29	1.55	4.14
8	1.71	4.83	1.57	5.02	1.89	4.83

Time to freeze

The effective thermal conductivities predicted by models which yielded results within the confidence limits of the experimental data can now be used to predict the time to freeze for an interlaced foam + water system.

This study focused on the effective thermal conductivity of a two phase system; the effective thermal conductivity of the solid-solid (foam+ice - single phase) system was not determined. However, if the assumption of heat transfer via conduction is valid, then the effective conductivity of any two component system, whether two phase or single phase, can be predicted by the above empirical models given that the structure of the system is equivalent and the relative ratio of thermal conductivities are comparable. Table 12 lists the predicted effective thermal conductivities of the water (liquid-solid) and ice (solid-solid) conditions for an arbitrary set of volume fractions. Since each of the three models; Asaad, Hadley, and De Vries relies only on the volume fractions of the phases, the number of conditions were reduced to reflect this. Volume fractions of 4, 6, and 8% are presented below.

Table 13. Estimated time to freeze for selected foam+water systems

Volume Fraction Solid, %	Asaad (hrs.)	Hadley (hrs.)	De Vries (hrs.)	Average (hrs.)
4	8.86	10.33	10.39	9.86
6	8.28	8.74	8.85	8.62
8	7.70	7.60	7.70	7.67

T_{start}=4.4°C
T_{end}=-17.8°C
$T_{freezer}$=-23°C
Container radius =16 cm

Using Equation [4], which was developed previously in the Background section, the time to freeze can be predicted for an interlaced system by substituting the conductivities of the fluid and solid phases of the material with the effective thermal conductivities predicted by the above models for a multi-component system. Table 13 presents the numerical data and Figure 41 shows the same data in a graphical format. The system parameters of container radius and start and end temperatures were held constant. These values are listed with the tabular data in Table 13.

From this data, the time to freeze is seen to reduce to with increasing volume fraction. At volume fractions of about 7 to 8% solid material, the time to freeze drops below the eight hour mark. This compares to the estimated time to freeze of a container of water-only to be over 17 hours. This point is significant because it suggests the use of an aluminum foam in the Direct Interface Fusible Heat Sink may reduce regeneration times by over half.

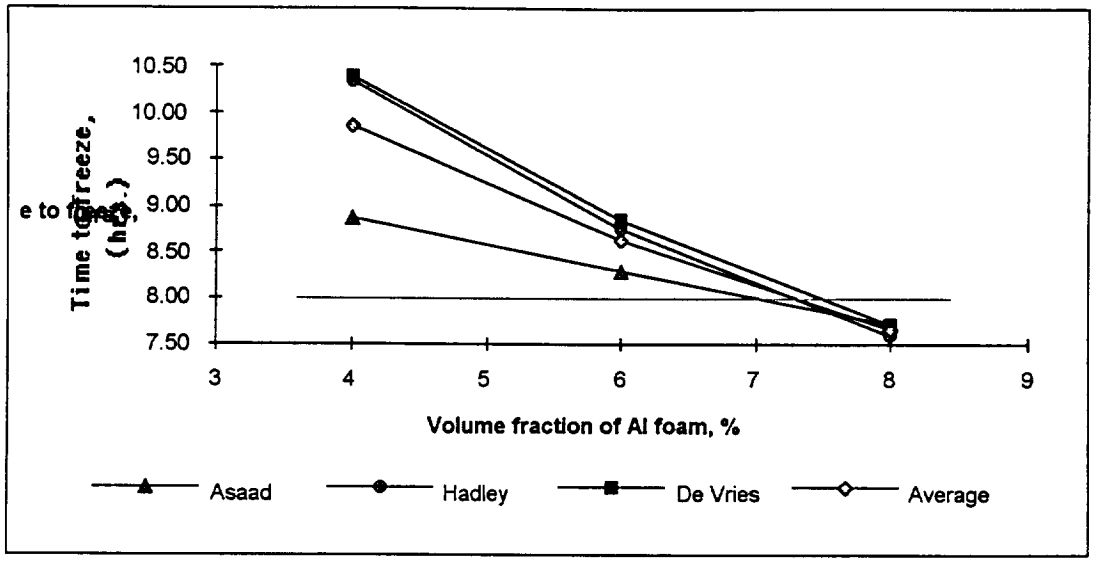

Figure 41. Estimated time to freeze as a function of volume fraction of added aluminum foam

While the reduction in regeneration time estimated here is not proven with direct experiment, the potential for significant time savings is encouraging. Future work in this area should concentrate on quantifying the true time savings when using an interlaced material over water alone.

In these past two sections the results obtained by experiment have been presented. The effective thermal conductivities of the foam+water specimens using the Transient Hot Strip method, plus the results of the volume fraction and pore size measurements were discussed. From these results it was concluded that the effective thermal conductivity increases with increases in the volume fraction of the foam phase. Changes in conductivity with pore size, on the other hand, was not statistically substantiated by the data. This effect was attributed to the large spread in pore size within the

samples and the overall size of the test population. A much larger sampling base may substantiate an effect of pore size on the effective conductivity.

The empirical models taken from the literature were compared to the experimental data and three models, authored by Asaad, Hadley, and De Vries, were found to predict the data to within the confidence intervals used. From these models, predictions to the regeneration, or freezing, rate were generated which indicated that the addition of a high conductivity material could decrease the regeneration time by as much as one-half. In a view towards future work, the actual time to freeze of a full-size DIFHS would be required to substantiate these claims.

Conclusion

This study examined the effect of volume fraction and pore size on the effective thermal conductivity of an aluminum foam and water system. Nine specimens of aluminum foam representing a matrix of three volume fractions (4-8% by vol.) and three pore sizes (2-mm) were tested with water as the matrix fluid to determine relationships with the effective thermal conductivity. It was determined that increases in volume fraction of the aluminum phase was correlated to increases in the effective thermal conductivity. It was not statistically possible to prove that changes in pore size of the aluminum foam correlated to changes in the effective thermal conductivity. However, interaction effects between the volume fraction and pore size of the foam were statistically significant. Ten theoretical models were selected from the published literature to compare against the experimental data. Models by Asaad, Hadley [1986], and de Vries provided effective thermal conductivity predictions within a 95% confidence interval.

References

1. G. Vogt, Ed., *Suited for Spacewalking*, NASA publication EP-279, NASA-Johnson Space Center, Houston, TX, March 1992

2. G. Vogt, Ed., *Information Summaries: Wardrobe for Space*, NASA publication PMS-033, NASA-Johnson Space Center, Houston, TX, July, 1989

3. Information found at: http://www.ksc.nasa.gov/shuttle/technology/sts-newsref/sts-apu.html#sts-eva

4. M. Diener and M. Balashov, Maintenance Practices on the EVA Suit 2000, *Aerospace Engineering*, SAE Publications, November 1994, pp. 7-10

5. P. Stone, J. Miles, S. Nair, C. Lomax, and B.W. Webbon, Tubular Evaporator Development for the PLSS, 1996 ICES Publication 961486, International Conference of Environmental Systems 1996, Monterey, CA 1996

6. J.L. Williams, B.W. Webbon, and R.J. Copeland, Advanced Extravehicular Protective Systems (AEPS) Study: Detailed Technical Notes, NASA-Ames Research Center, Moffett Field, CA, March 1972

7. C. Lomax and B.W. Webbon, "A Direct-Interface Fusible Heat Sink For Astronaut Cooling", NASA Technical Memorandum 102835, NASA-Ames Research Center, Moffett Field, CA, May 1990

8. C. Lomax and B. Kader, Direct-Interface Fusible Heat Sink Performance Tests, ICES Publication 941384, International Conference On Environmental Systems 1994, Friedrichshafen, Germany, 1994

9. Extravehicular Activity Systems Project Plan: Human Support Technology Thrust Exploration Technology Program, NASA-Ames Research Center, Moffett Field, CA, April 1991

10. J. Moskito, C. Lomax, and G. Selvaduray, Effective Thermal Conductivity of Interlaced Materials, ICES Publication # 951636, International Conference On Environmental Systems 1995, San Diego, CA, 1995

11. W. Woodside and J.H. Messmer, Thermal Conductivity Of Porous Media I. Unconsolidated Sands, *Journal Of Applied Physics*, vol. 32, no. 9, September 1961, pp. 1688-1698

12.* P.G. Collinshaw and J.R.G. Evans, An Assessment of Expressions for the Apparent Thermal Conductivity of Cellular Materials, ???,

13. Information found at: http://www.ksc.nasa.gov/shuttle/technology/sts-newsref/sts-apu.html#sts-wsb

14. M. Dubois, B. Mullender, S. Van Oost, J. Druart, w. Supper, and D. Titterton, Space Qualification of High Capacity Grooved Heat Pipes, ICES Publication 951551, International Conference On Environmental Systems 1995, San Diego, CA, 1995

15. B. Moschetti and E. Voyer, Development of a High Performance Heat Pipe (HPHP) for a Satellite Application, ICES Publication 951552, International Conference On Environmental Systems 1995, San Diego, CA, 1995

16. J. Moskito, Analysis of the Vapor Flow in a Tubular Boiler heat Exchanger, Unpublished, 1995

17. K. Lundsford, Flow Across and Inside of a Membrane Tube, MS Thesis, MAE Dept., University-Columbia, 1997

18. W. Schneider, Vapor Flow Through a Porous Membrane- A Throttling Process with Condensation and Evaporation, Acta Mechanica, vol. 47, 1983, pp. 15-25

19. D. Pitts and L. Sissom, Theory and Problems of Heat Transfer, McGraw-Hill Publishers, New York, 1977

20. Duocel Ceramic Foam, Sales Literature, Energy Research and Generation, Inc., Oakland, CA, 1995

21. Reticulated Vitreous Carbon, Sales Literature, Energy Research and Generation, Inc., Oakland, CA, 1995

22. D. A. Zumbrennen, R. Viskanta, and F.P. Incopera, Heat Transfer Through Porous Solids with Complex Internal Geometries, *International Journal of Heat and Mass Transfer*, vol. 29, no. 2, pp. 275-283

23. Duocel Aluminum Foam, Sales Literature, Energy Research and Generation, Inc., Oakland, CA, 1995

24. B. Leyda, ERG Inc., Private Conversation September 19, 1996

25. F.B. Nimick and J.R. Leith, A Model for Thermal Conductivity of Granular Porous Media, *Journal of Heat Transfer*, 114, May 1992, pp. 505-508

26. G.R. Hadley, Thermal Conductivity Of Packed Metal Powders, *International Journal Of Heat and Mass Transfer*, vol. 29, no. 6, 1986, pp. 909-920

27. Y. Asaad, A Study of the Thermal Conductivity of Fluid-Bearing Porous Rocks, Ph.D. Thesis, University of California, Berkeley, CA, 1995

28. A.V. Luikov, A.G, Shashkov, L.L. Vasiliev, and Yu, E. Fraiman, Thermal Conductivity Of Porous Systems, *International Journal Of Heat And Mass Transfer* , vol.. 11, 1968 pp. 117-140

29. G.N. Dulnev, D.P. Volkov, and V.I. Malarev, Thermal Conductivity of Moist Porous Materials, *Journal of Engineering Physics (English translation of Inzhenerno-Fizicheskii Zhurnal)*, vol. 56, no. 2, February, 1989, pp. 198- 206

30. H. Bjurstrom, E. Karawacki, and B. Carlsson, Thermal Conductivity of a Microporous Particulate Medium: Moist Silica Gel, *International Journal of Heat and Mass Transfer*, 27, 11, 1984, pp. 2025-2036

31.*

32. *Standard Test Method For Thermal Conductivity Of Liquids*, ASTM D2717-90, American Society for Testing and Materials, Philadelphia, PA, 1990

33. *Standard Test Method For Thermal Conductivity Of Solids By Means Of The Guarded Comparative Longitudinal Heat Flow Technique*, ASTM E1225-87, American Society for Testing and Materials, Philadelphia, PA, 1987

34. ASTM E1530 Guarded Heat Flow Meter Method, Technical Note 50, Anther Corp., Pittsburgh, PA, 1995

35. G. Sheffield and J.R. Schorr, Comparison of Thermal Diffusivity and Thermal Conductivity Methods, *Ceramic Bulletin*, vol. 70, no. 1, 1991, pp. 102-106

36. T. Ashworth, E. Ashworth, and S.F. Ashworth, A New Apparatus for Use with Materials of Intermediate Conductivity, International Thermal Conductivity Conference (21st), Lexington , KY, 15-18 Oct 1989 pp. 229-241

37. N. Moore, H. Wolf, and F.K. Deaver, Simultaneous Heat and Mass Transfer in Moist Porous Media, University of Arkansas, Fayetteville, AR, 1972

38. R. Singh, N.S. Saxena, and D.R. Chaudhary, Simultaneous Measurement Of Thermal Conductivity And Thermal Diffusivity Of Some Building Materials Using The Transient Hot Strip Method., *Journal Of Physics D: Applied Physics*, vol. 18, 1985, pp. 1-8

39. S.E. Gustafsson, E. Karawacki, and M.N. Khan, Transient Hot-Strip Method For Simultaneously Measuring Thermal Conductivity And Thermal Diffusivity Of Solids And Fluids. *Journal Of Physics D: Applied Physics*, vol. 12, 1979 pp. 1411-1421

40. S.E. Gustafsson, E. Karawacki, M.A. Chohan, Thermal Transport Studies Of Electrically Conducting Materials Using The Transient Hot-Strip Technique, *Journal Of Physics D; Applied Physics*, vol. 19 1986 pp. 727-735

41. P. Andersson and G. Backstrom, Thermal Conductivity Of Solids Under Pressure By The Transient Hot Wire Method, *Review Of Scientific Instruments*, vol. 47, no. 2, Feb. 1976, pp. 205-209

42. C.W. Kistler and J. Homeny, Hot Wire Thermal Conductivity Test System, Presentation Notes, Orton Refractories Testing and Research Center, Westerville, OH, 1993

43. *Standard Test Method For Thermal Conductivity Of Refractories by Hot Wire (Platinum Resistance Thermometer technique)* ASTM C1113-90, American Society for Testing and Materials, Philadelphia, PA, 1990

44. J.C. Wilshee, Comparison of Thermal Conductivity Methods, *Proceedings of the British Ceramic Society*, 29, 1980, pp. 153-173

45. D.G. Cahill, and R.O. Pohl, Thermal Conductivity Of Amorphous Solids Above The Plateau, *Physical Review B*, vol. 35, no. 8, 1987, pp. 4067-4073

46. H.G. Jensen, Kolrausch Heat Conductivity Apparatus for Intermediate or Advanced Laboratory, American *Journal of Physics*, vol. 38, no. 7, 1970, pp. 870-874

47. K. Bala, P.R. Pradhan, N.S. Saxena, and M.P. Saksena, Effective Thermal Conductivity Of Copper Powders, *Journal of Physics D, Applied Physics*, vol. 22, 1989, pp. 1068-1072

48. N.S. Saxena, M.A. Chohan and S.E. Gustafsson, Effective Thermal Conductivity Of Loose Granular Materials, *Journal Of Physics D: Applied Physics*, vol. 19, 1986, pp. 1625-1630

49.*

50. M. Abramowitz and I.A. Stegun, Handbook of Mathematical Functions with Formulas, Graphs, and Mathematical Tables, National Bureau of Standards, Applied Mathematics Series 55, 1964 pg. 231

51. *Standard Test Method For Determining Average Grain Size* , ASTM E112-88, American Society for Testing and Materials, Philadelphia, PA, 1988

52. E.E. Underwood, Quantitative Metallography, *ASM Metals Handbook, Volume 9, 9th Ed.*, ASM, Metals Park, OH, 1989, pp. 124-134

53. Log, Metallinou Thermal Conductivity Measurements Using A Short Transient Hot Strip Method, *Review Of Scientific Instruments*, vol. 63, no. 8 1992, pp. 3966-3971

54. Taple, Bekeris, Sanchez, Simonelli Reduction Of Radiation Errors In Thermal Conductivity Measurements Above 100k, *Review Of Scientific Instruments*, vol. 62, no. 4, April 1991, pp. 1054-1056

55. W. Mendenhall and T. Sincich, *Statistics for Engineers and the Sciences, 4th ed.*, Prentice -Hall, New Jersey, 1995, pg. 569-582